Miner Petrol (2015) 109:531–553
DOI 10.1007/s00710-015-0391-5

ORIGINAL PAPER

Orogenic-type copper-gold-arsenic-(bismuth) mineralization at Flatschach (Eastern Alps), Austria

Johann G. Raith[1] · **Thomas Leitner**[3] · **Werner H. Paar**[2]

Received: 1 April 2014 / Accepted: 1 June 2015 / Published online: 16 June 2015

Abstract Structurally controlled Cu-Au mineralization in the historic Flatschach mining district (Styria, Austria) occurs in a NE–SW to NNE–WSW oriented vein system as multiple steep-dipping calcite-(dolomite)-quartz veins in amphibolite facies metamorphic rocks (banded gneisses/amphibolites, orthogneisses, metagranitoids) of the poly-metamorphosed Austroalpine Silvretta-Seckau nappe. Vein formation postdated ductile deformation events and Eoalpine (Late Cretaceous) peak metamorphism but predated Early to Middle Miocene sediment deposition in the Fohnsdorf pull-apart basin; coal-bearing sediments cover the metamorphic basement plus the mineralized veins at the northern edge of the basin. Three gold-bearing ore stages consist of a stage 1 primary hydrothermal (mesothermal?) ore assemblage dominated by chalcopyrite, pyrite and arsenopyrite. Associated minor minerals include alloclasite, enargite, bornite, sphalerite, galena, bismuth and matildite. Gold in this stage is spatially associated with chalcopyrite occurring as inclusions, along re-healed micro-fractures or along grain boundaries of chalcopyrite with pyrite or arsenopyrite. Sericite-carbonate alteration is developed around the veins. Stage 2 ore minerals formed by the replacement of stage 1 sulfides and include digenite, anilite, "blue-remaining covellite" (spionkopite, yarrowite), bismuth, and the rare copper arsenides domeykite and koutekite. Gold in stage 2 is angular to rounded in shape and occurs primarily in the carbonate (calcite, Fe-dolomite) gangue and less commonly together with digenite, domeykite/koutekite and bismuth. Stage 3 is a strongly oxidized assemblage that includes hematite, cuprite, and various secondary Cu- and Fe-hydroxides and -carbonates. It formed during supergene weathering. Stage 1 and 2 gold consists mostly of electrum (gold fineness 640–860; mean=725; n=46), and rare near pure gold (fineness 930–940; n=6). Gold in stage 3 is Ag-rich electrum (fineness 350–490, n=12), and has a high Hg content (up to 11 mass %). The Cu-Au deposits in the Flatschach area show similarities with meso- to epizonal orogenic lode gold deposits regarding the geological setting, the structural control of mineralization, the type of alteration, the early (stage 1) sulfide assemblage and composition of gold. Unique about the Flatschach district is the lower-temperature overprint of copper arsenides (domeykite and koutekite) and copper sulfides (djurleite, yarrowite/spionkopite) on earlier formed sulfide mineralization. Based on mineralogical considerations temperature of stage 2 mineralization was between about 70 °C and 160 °C. Gold was locally mobilized during this low-temperature hydrothermal overprint as well as during stage 3 supergene oxidation and cementation processes.

Editorial handling: A. Beran

Electronic supplementary material The online version of this article (doi:10.1007/s00710-015-0391-5) contains supplementary material, which is available to authorized users.

✉ Johann G. Raith
johann.raith@unileoben.ac.at

Thomas Leitner
leitho@gmx.at

Werner H. Paar
paarwerner@aon.at

[1] Department of Applied Geosciences and Geophysics, Montanuniversitaet Leoben, Leoben, Austria

[2] Pezoltgasse 46, A-5020 Salzburg, Austria

[3] Salinen Austria AG, Bad Aussee, Austria

Introduction

Mining of gold and silver has a century-long history in the Alps. Dozens of historic mine sites and hundreds of showings in Austria (e.g., see IRIS data-base, Weber 2015) document

the previous importance of gold mining in the Alps but also indicate the potential of the Alpine orogen for precious metals mineralization (Fig. 1a). The majority of gold deposits in the Eastern Alps in Austria are located in the Hohe Tauern area; i.e., in the Penninc units of the Tauern Window and in the Austroalpine units to its south, but there also exist Au-Ag-base metal deposits in the Austroalpine tectonic units further to the east in the Niedere Tauern and Saualpe area (Figs. 1a).

The Cu-Au deposits north of Flatschach (community of Schönberg)—the object of this study—represent one of these former mining areas. Mining there goes back to the 15th century; the most active period of mining was in the 18th century. These deposits were re-investigated after World War II (Friedrich 1964; Jarlowsky 1951) and explored in the seventies to eighties of the 20th century (Göd 1987; Punzengruber et al. 1977). Since 2011 this region attained renewed interest from an exploration point of view when Noricum Gold started to re-evaluate the potential for gold and copper of these deposits (Noricum Gold Limited 2014). Some geological and mineralogical results of the concommitant resarch project of this exploration activity are presented in this paper.

A peculiar feature of these deposits is the association of gold with a variety of copper sulfides and the rare copper arsenides domeykite and koutekite which is atypical for orogenic-type gold deposits.

This study presents data on the geological setting and ore mineralogy of these deposits. It focuses on the different mineral assemblages containing gold and its association with copper arsenides and copper sulfides. Furthermore, constraints on the temperatures of formation as deduced from ore assemblages are discussed and a comparison with gold deposits of undoubted orogenic origin in the Eastern Alps is made. General aspects of orogenic and intrusion-related gold deposits are compared to Flatschach in order to correctly classify these deposits and clarify their relation to the regional geological evolution of the Alps. Results of this paper are hopefully of interest to researchers who work on various aspects of gold deposits in orogenic belts including those interested in processing polymetallic gold ores.

Geology

Regional geological setting

The study area is located in the Austroalpine basement units of the Eastern Alps to the east of the Penninic Tauern Window (Fig. 1a, b). The Austroalpine tectonic units include metamorphic basement nappes plus sedimentary cover sequences of the upper (Adriatic) plate that were thrust onto Penninic units and the lower plate European continental margin during the Alpine orogeny (Schmid et al. 2004). The Austroalpine units are subdivided into (1) Lower Austroalpine nappes, (2) the Upper Austroalpine Northern Calcareous Alps and Greywacke Zone, and (3) the Upper Austroalpine basement nappes (Fig. 1b; Schmid et al. 2004). Using this classification, the Flatschach area is located in the Silvretta-Seckau and the Koralm-Wölz nappe systems of the Upper Austroalpine basement. The Neogene pull-apart Fohnsdorf basin and the corresponding strike-slip fault system are the youngest geological units / structures in the area (Fig. 1a, b).

Silvretta-Seckau nappe system

The Silvretta-Seckau nappe system is the deepest Upper Austroalpine tectonic unit. It is composed of polymetamorphic basement rocks (up to few km thick) and a thin cover of post-Variscan Late Paleozoic to Mesozoic sediments (Rannach Formation). The dominant metamorphic rocks of this nappe system are biotite-plagioclase gneisses (locally hornblende-bearing and migmatitic) and amphibolites; the latter are associated with metagabbros and serpentinized ultramafic rocks. The magmatic protoliths of these rocks formed due to subduction, collision and extensional processes from the Late Proteozoic to Ordovician (Neubauer et al. 2002). Acid to intermediate plutonitic protoliths were transformed to metagranitoids derived from calc-alkaline I-type granitoids of Variscan age (Schermaier et al. 1997) but also including S-type granites in its uppermost sections (Pfingstl et al. 2015). Two Rb-Sr whole rock isochron ages for leucocratic orthogneisses yielded 354±16 and 432±16 Ma, respectively (Scharbert 1981), indicating that Variscan as well as pre-Variscan rocks are present in the eastern part of the Seckau Silvretta nappe system.

A zone of intermixed rocks (Gaaler Schuppenzone) including tectonic slices of the Permo-Triassic cover (Rannach Formation) forms the NW continuation of the upper Speik Complex. This complex is mainly composed of banded amphibolites and hornblende-bearing paragneisses, meta-ultramafic rocks, metagabbros and locally retrograde eclogites. In the hanging wall marbles, calc-silicate rocks and micaschists become more common. Meta-ultramafic rocks are primarily found toward the base of the complex below the amphibolite-dominated part. The Speik Complex is interpreted as a dismembered ophiolite of pre-Alpine age (Neubauer et al. 1989) that formed in a supra-subduction regime during the Late Proterozoic to Cambrian (~750 to ~550 Ma, Melcher and Meisel 2004). The Rb-Sr whole rock isochron age of 331±25 Ma for the augengneisses (Frank et al. 1983) can be interpreted as the emplacement age of the granitic protoliths, which intruded the older series during the Variscan orogeny in the Lower Carboniferous.

Conditions of Eoalpine metamorphism in the Permomesozoic Rannach Formation were estimated at 530-550 °C, 0.8-0.9 GPa (Faryad et al. 2002). The pressure-

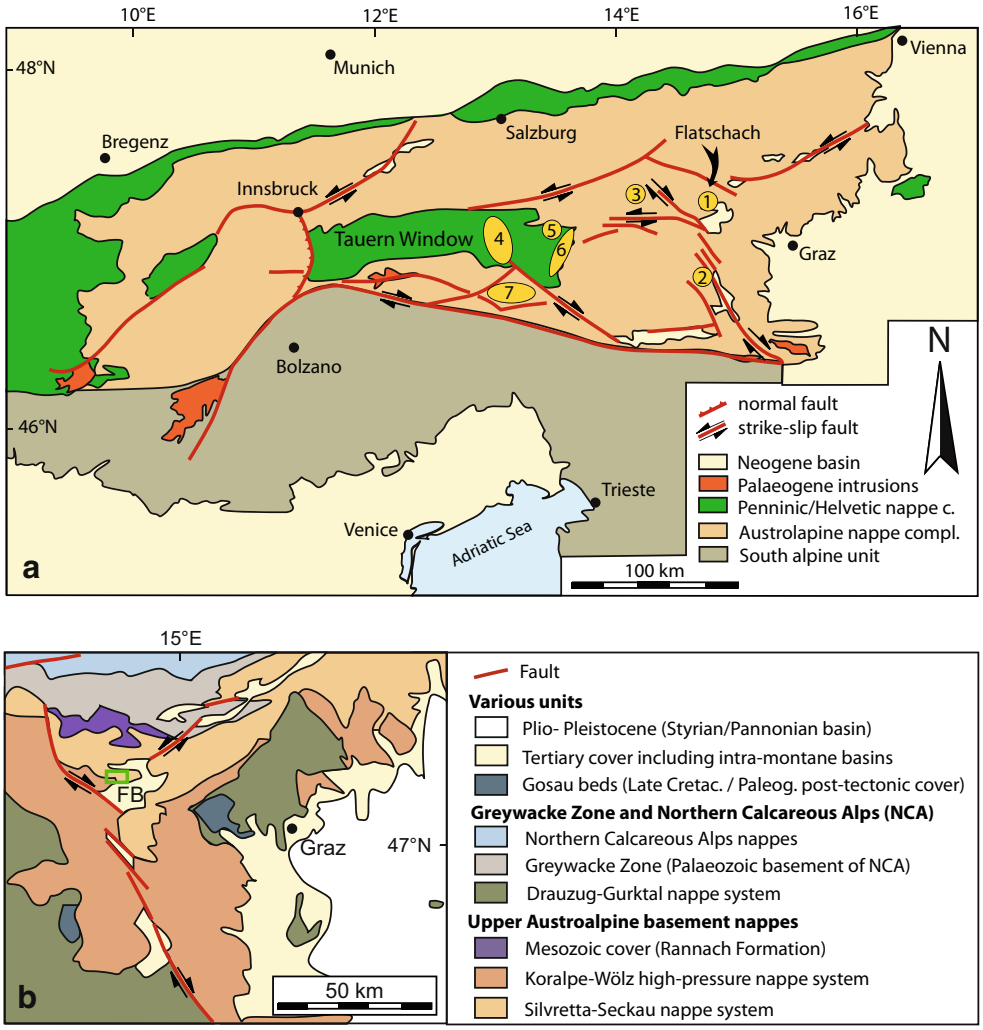

Fig. 1 **a** Geological map of the eastern part of the Alps showing main tectonic / geological units, structures and locations of gold deposit districts in Austria. *1* Flatschach; *2* Kliening; *3* Pusterwald; *4* Gastein-Rauris; *5* Rotgülden; *6* Schellgaden; *7* Kreuzeck- and Goldeck Mountains (after Amann et al. 2002) **b** Geological sketch map showing location of the study area (*green box*) in the context of regional major tectonic/ geological units (simplified after Schmid et al. 2004). FB Fohnsdorf basin

temperature conditions of pre-Alpine high-pressure metamorphism are 700 °C, 1.8–2.2 GPa and an Ar-Ar age of high-pressure amphiboles yielded an age of ~400 Ma (Faryad et al. 2002). The Rb-Sr ages of biotite in the Seckau Complex range from 76 Ma to 86 Ma; they are interpreted as cooling ages of Eoalpine metamorphism and linked with extension-relatd exhumation of the Seckau nappe in the Late Cretaceous (Pfingstl et al. 2015).

Koralpe-Wölz nappe system

The Koralpe-Wölz nappe system tectonically overlies the Silvretta-Seckau nappe system, and consists of several nappes, which all record the same Eoalpine deformation and metamorphic history. The metamorphic gradient of the units increases from the northern (greenschist facies) to the southern central units (upper amphibolite/eclogite facies); metamorphic grade also decreases from the basal central units towards the hanging wall units. The rocks record poly-metamorphic orogenic metamorphism. In addition to Eoalpine medium to high-pressure Barrovian metamorphism, some units preserve evidence of low-pressure metamorphism and granitoid and pegmatite emplacement of Permian age (Schuster and Stüwe 2008; Thöni 1999).

The dominant lithologies of the Koralpe-Wölz nappe system are poly-deformed phyllites, garnet micaschists or aluminium silicate-bearing gneisses. Marbles, amphibolites and quartzites are locally intercalated. In the Flatschach area, the Koralpe-Wölz nappe system is represented by micaschists of the Wölz Complex in the southern part of the field area (Fig. 2). Light colored garnet micaschists in this complex contain white mica, quartz and minor albite, garnet, biotite and chlorite. The oldest garnet generation in metapelites of the Wölz Complex formed during the low-pressure event (0.4–0.5 GPa, 540–560 °C, Bestel et al. 2009) in the Permian (~270 Ma, Schuster and Stüwe 2008). The garnet rims and the smaller garnets in the northern micaschists crystallized during the Upper Cretaceous (~90 Ma) under P–T conditions of 0.7–0.8 GPa and 550–570 °C (Bestel et al. 2009). The widespread K-Ar muscovite and Rb-Sr biotite ages between

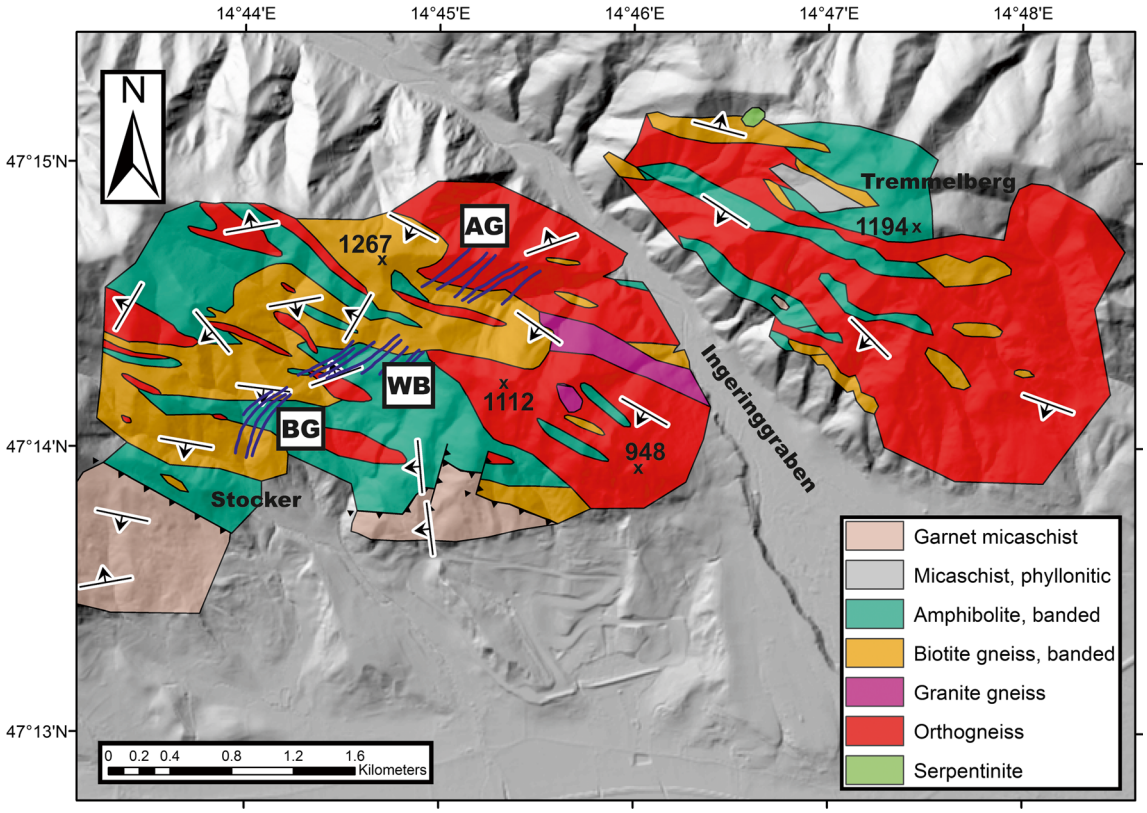

Fig. 2 Geological map based on 1:10,000 scale re-mapping of Flatschach – Tremmelberg area (Leitner 2013). Location of the main veins (*blue lines*) in the three historic mining districts (BG Brunngraben, WB Weissenbach, AG Adlitzgraben) is taken from Jarlowsky (1951). LIDAR basemap from GIS Steiermark. Neogene cover not shown

~80 and 90 Ma are evidence that the predominant metamorphic event in the Koralpe-Wölz nappe system is Eoalpine (Thöni 1999).

The Neogene Fohnsdorf-Seckau basin

Sediments of the Neogene Fohnsdorf basin cover the Austrolapine basement rocks in the southernmost study area (see e.g., Sachsenhofer et al. 2000; Strauss et al. 1999). This ~20 km^2 large and up to 2000 m thick basin formed in the Miocene as result of orogen-parallel extension and lateral extrusion of the central parts of the Eastern Alps to the east. The asymmetric basin developed between major sinistral and dextral wrench faults and is one of several en-echelon basins along the Mur-Mürz fault system. The basin is located at the junction of the sinistral ENE-trending Mur-Mürz fault system and the dextral NW-trending Pöls-Lavanttal fault system (Fig. 1a, b). The three main sedimentary formations of this intra-montane basin are composed of various clastic sediments and contain coal deposits at its base. Sediments aong the northern basin margin were deposited onto the basement rocks between the Early to Middle Miocene (Badenian?).

Regional faults can be assigned to four brittle deformation phases. During the pre-Miocene, the NW-SE trending Ingering strike-slip fault formed. The other three phases are related to Miocene basin evolution. The first phase is the pull-apart phase related to sinistral strike-slip faulting, the second one coincided with subsequent fault reactivation and half-graben formation, and the third one was related to further post-sedimentary compression (Strauss et al. 2001).

Local geology

Eight ore veins—of these three are regarded as main ones—are known in the three mining districts referred to as Brunngraben, Weissenbach and Adlitz mining districts ("Revier", Fig. 2). In the Weissenbach and Adlitz mining districts the set of veins strikes NE-SW with a dip of 70–80° to the NW. In the Brunngraben mining district in the SW the veins become oriented NNE–SSW with a dip of 72–76° to the SE (Friedrich 1964; Jarlowsky 1951). The veins are up to ~1 m wide and are partly filled with fault gouge material derived from cataclasis of the surrounding host rocks, which are locally hydrothermally altered and converted into argillaceous material. Thin phyllosilicate-rich selvages border the veins. Copper-gold mineralization within the veins occurs in disseminated form, in patches or in bands. Quartz and calcite are the main gangue minerals. The upper mine levels and the southern mine districts are reported to be enriched in

arsenopyrite and pyrite, whereas chalcopyrite increases with depth and becomes the predominant sulfide in the north (Jarlowsky 1951). Coal-bearing sediments of the Neogene Fohnsdorf basin unconformably overlie the ore veins in the today inaccessible Fortuna Unterbau gallery (Jarlowsky 1951). This observation is important because it constrains the mineralized structures to be of pre-Miocene age.

During a geological field campaign in 2012 the Flatschach-Tremmelberg area was remapped on a 1:10,000 scale (Leitner 2013). The dominant host rocks to the mineralized veins are amphibolites, biotite gneisses and orthogneisses. Micaschists, granite gneiss and serpentinite are subordinate. Amphibolites and biotite gneisses are commonly banded and interlayered on various (from decimetre to metre) scales. They are summarized as *amphibolite-biotite gneiss unit.* The amphibolites are massive to foliated, fine- to medium-grained and composed of hornblende and plagioclase with minor quartz, biotite, ±garnet, ±muscovite, ±clinozoisite, ±ilmenite. Thin veinlets and disseminations of scheelite accompanied by tourmaline and hosted in the amphibolites were encountered during the exploration drilling campaign at the Weissenbach district (Paar 2014).

Biotite gneisses are well foliated and composed of plagioclase, alkali feldspar, quartz, biotite, muscovite, garnet, ±hornblende, ±epidote and±chlorite. The modal compositon of these gneisses varies considerably; biotite-gneiss, biotite-muscovite gneiss, garnet-biotite-muscovite gneiss as well as quartzo-feldspathic varieties can be distinguished. Due to these petrographic variation and small-scale interlayering of the various lithologies, the amphibolite-biotite gneiss unit is interpreted as a volcano-sedimentary unit with a contribution of plutonic material.

Light-colored medium to coarse-grained feldspar-rich orthogneisses contain variable amounts of alkali feldspar, plagioclase, quartz, muscovite, with minor biotite and tourmaline Dark biotite-rich and fine-grained mylonitic varieties also occur along with epidote-hornblende and tourmaline-rich gneiss. Locally, coarser grained (up to 10 mm) *granite gneiss* is interlayered with the orthogneisses, especially to the south of Adlitzgraben (Fig. 2). It has a rather homogeneous composition with major alkali feldspar, plagioclase and quartz, and minor muscovite±biotite.

Rare, small lenses of *serpentinite* occur at Tremmelberg and contain serpentine-group minerals, olivine, magnetite, chlorite and carbonates. Pyrite, chalcopyrite, bornite, covellite and millerite are accessory sulfides.

The *garnet micaschists* belonging to the Wölz-Koralpe nappe system include silver–grey schists, which are dominated by muscovite and normally contain mm–cm sized garnet porphyroblasts. Larger garnets may show two growth stages. Quartz, biotite, chlorite and feldspars are minor constituents. Near the thrust zone where the micaschists are in tectonic contact with the underlying amphibolites of the Seckau-Silvretta nappe system, the micaschists tend to contain more chlorite.

Structural measurements are summarized in Fig. 3. The poles of foliation planes in the host rocks of the veins are distributed along a ~N–S trending girdle (π - circle 098/70) in the stereographic projection diagram (Fig. 3a). The calculated π - point (Δ1; 278/20, Fig. 3a) gives the calculated fold axis point of this great circle and fits well with the maximum of the measured fold axes and other lineations in the mapped area (Fig. 3b). The majority of the lineations are oriented WNW-ESE with a predominant flat plunge to ~W to WNW orientation. The data reflect a regional scale re-folding of the major foliation. All these formed during the regional amphibolite facies metamorphism of Eoalpine age.

Data of brittle structures are shown in Figs. 3c, d. The measured fault planes show N-S to WSW-ENE orientation, however, with a considerable scatter of the data. A main fault orientation is between NNW/NW and SSW/SW with a dip of 60 to 90°. This direction corresponds to the orientation of the mineralized Cu-Au veins (see Fig. 2). Two major directions, NNW-SSW and WNW-ESE, become visible in the joint planes data set; i.e., these steeply dipping joint planes belong to a conjugate joint system.

From field observations and structural data, it is clear that the mineralized Cu-Au veins post-date the ductile deformation event(s). Orientation of the ore veins approximately corresponds with the regional orientation of one set of the fault planes and also with the dominant set of unmineralized late joints. It is therefore suggested that the mineralized vein system formed after the main ductile deformation stage (but prior to the brittle joints) in a regional stress regime characterized by NNE-SSW compression with a WNW-ESE extensional component.

Sampling and methods

The total sample set studied includes material collected from fieldwork in 2012 as well as archive material from previous projects (electronic supplementary material appendix 1). In the first project phase, a total of 22 polished sections were investigated. This material is mainly from the Weissenbach mining district (Fig. 2). In the second project phase, a total of 29 polished sections were investigated. These sections are mostly from the PhD thesis by Jarlowsky (1951) ("Friedrich Archiv") and were provided by Universalmuseum Joanneum Graz. Three new samples collected during sampling of dumps at Barbara adit in April 2012 were added to this sample set. The total material investigated is from all three mining districts in the Flatschach area; i.e., Brunngraben, Weissenbach and Adlitzgraben (Fig. 2).

Polished sections (40 respectively 30 mm in diameter) were used for reflected light microscopy. A Zeiss AXIO

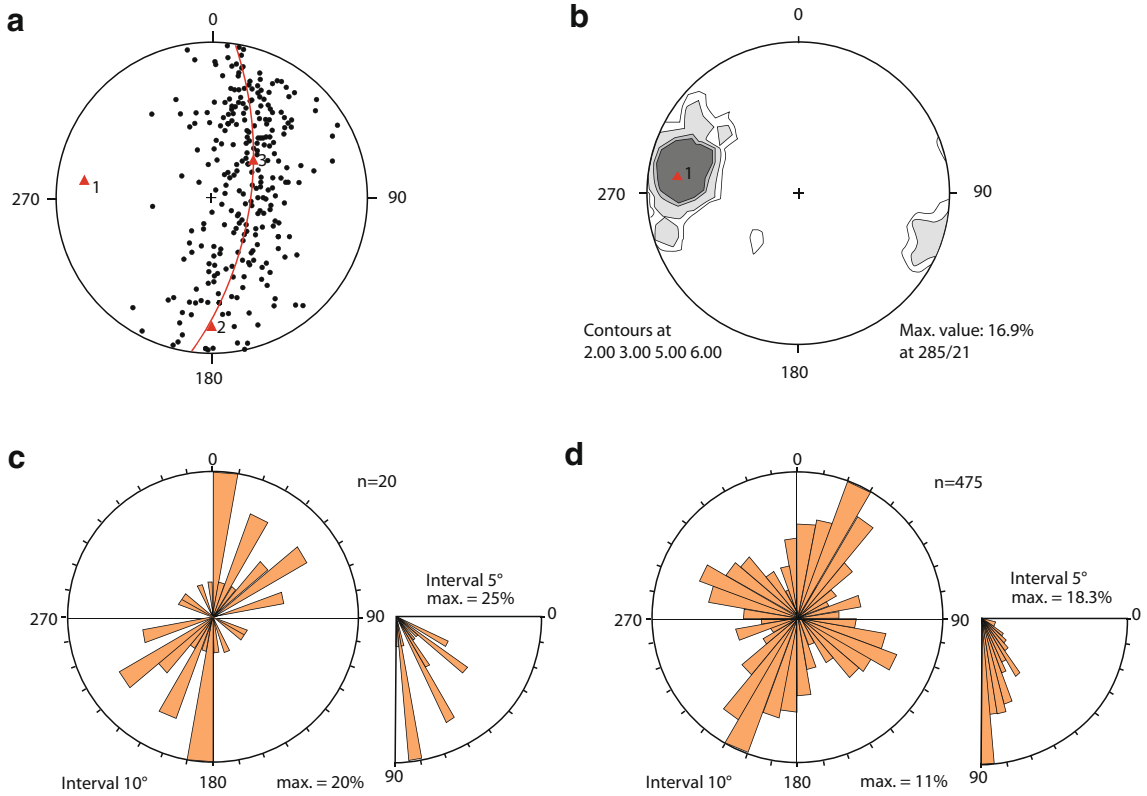

Fig. 3 **a** Lower hemisphere, equal area plot showing pole points of the foliation planes in the host rocks of the veins; the *red line* shows the constructed π - *circle*, point 1 (*red triangle*) defines the constructed fold-axis. **b** Lower hemisphere, equal area plot showing contour plot of lineations. **c** Rose diagram of fault planes. Orientation of mineralized Cu-Au quartz veins corresponds to the smaller population (~NE-SW oriented). **d** Rose diagram of joint planes. Two main directions, both steeply dipping, are visible (NNW-SSW and WN-ESE). All diagrams were constructed using the tectonics FP software (Reiter and Acs http://www.tectonicsfp.com)

Scope.A1 polarization microscope equipped with a Zeiss AXIO Cam ERc 5 s digital camera and AxioVision Rel.4.8.2.0 software was used for transmitted and reflected light microscopy. The electron microprobe analyses (EMPA) were done at the Eugen Stumpfl Electron Microprobe Laboratory of Universitätszentrum Angewandte Geowissenschaften Steiermark (UZAG) at Montanuniversitaet Leoben. The analyses were made by wavelength dispersive spectrometry (WDS) using a JEOL JXA 8200 Superprobe. The analytical conditions were: acceleration voltage 20 kV, probe current 15 nA or 10 nA. Kα lines were used for analyzing Fe, Cu, and S, Lα lines for Ag, Au, Sb and As and Mα lines for Hg, Pb and Bi. Calculated detection limits (95 % confidence, in ppm) are about: Fe (120), Cu (180) and S (150), Ag (180), As and Au (800), and about 1800 ppm for Sb, Hg, Pb and Bi. Natural mineral standards were used for calibration. Some analyses of small grains (<10 μm) may show effects of the surrounding matrix and give too low totals.

The Raman spectra of some phases were measured with an ISA JobinYvon LABRAM confocal Raman spectrometer, using a frequency-doubled 120 mW Nd-YAG laser with an excitation wavelength of 532 nm. Silicon and polyethylene were used for calibration. The spectra were collected between 180 and 2000 cm^{-1} with a resolution of approximately ±2 cm^{-1}. To allow phase identification the measured spectra were compared with spectra reported in the RRUFF database (RRUFF 2013) and an in-house database. If available, abbreviations of mineral names as suggested by Whitney and Evans (2010) were used (Table 1).

Mineralogy

Vein mineralogy and wall rock alteration

Because of the inaccessibility of most of the historic underground mine workings and poor exposures, hydrothermal alteration could not be studied in outcrop. Information comes from larger blocks taken at dumpsites. Sample T.03 is from a block taken at the dumps of Barbara adit. In this sample, sulfide mineralization is found in the form of sulfide-bearing quartz-calcite veinlets surrounded by altered host rock (Fig. 4a, b).

The major minerals within the veinlets are quartz, calcite and chalcopyrite, arsenopyrite and minor pyrite. Gold was not

Table 1 Ore and gangue minerals identified in this study. The mineral names and the nominal mineral formulae are given. When available abbreviations according to Whitney and Evans (2010) are used; for Cu sulfides nominal formulae as well as on basis of *S*=1 are listed

Mineral	Abbreviation	Chemical composition	Frequency
Cu-S minerals			
Chalcocite	Cct	Cu_2S	x
Digenite	Dg	$Cu_{1.8+x}S$; Cu_9S_5	xx
Djurleite	Dju[a]	$Cu_{1.94}S$; $Cu_{31}S_{16}$	x
Anilite	Ani[a]	$Cu_{1.75}S$, Cu_7S_4	xx
Geerite	Gee[a]	$Cu_{1.6}S$; Cu_8S_5	x
Spionkopite "(bb. covellite") [b]	Cv / Spk[a]	$Cu_{1.39}S$; $Cu_{39}S_{28}$	xx
Yarrowite ("bb. covellite") [b]	Cv/ Yar[a]	$Cu_{1.13}S$; Cu_9S_8	xx
Cu-As minerals			
Domeykite	Dom[a]	$Cu_{3-x}As$, x=0.02 – 0.4	xx
Koutekite	Kou[a]	Cu_5As_2	x
Other ore minerals			
Alloclasite ?	Alc[a]	$Co_{1-x}Fe_xAsS$ (low Ni content)	x
Arsenopyrite	Apy	FeAsS	xxx
Bismuthinite	Bis[a]	Bi_2S_3	x
Bornite	Bn	Cu_5FeS_4	x
Chalcopyrite	Ccp	$CuFeS_2$	xxx
Enargite	Eng	Cu_3AsS_4	x
Galena	Ga	PbS	x
Matildite	Mat[a]	$AgBiS_2$	x
Bismuth	Bi	Bi	xx
Copper	Cu	Cu	x
Gold, electrum	Au	Au; (Au,Ag)	x
Pyrite	Py	FeS_2	xxx
Safflorite	Saf[a]	$(Co,Fe,Ni)As_2$	x
Sphalerite	Sp	ZnS	x
Tetrahedrite	Ttd	$Cu_{12}As_4S_{13}$ - $Cu_{12}Sb_4S_{13}$	x
Xenotime	Xtm	$Y(PO_4)$	x
Cuprite	Cpr	Cu_2O	x
Hematite	Hem	Fe_2O_3	xx
Magnetite	Mag	Fe_3O_4	x
Ilmenite	Ilm	$FeTiO_3$	x
Non-ore minerals			
Azurite	Azu[a]	$Cu_3(CO_3)_2(OH)_2$	x
Calcite	Cal	$CaCO_3$	xxx
Calcite, Fe-rich[c]			xx
Chlorite	Chl	$(Fe,Mg,Al,Zn)_6(Si,Al)_4O_{10}(OH)_8$	xx
Dolomite/Ankerite	Dol/Ank	$Ca(Mg,Fe)(CO_3)_2$	xxx
Fe - hydroxides (limonite)	Lim	FeO(OH).nH2O	xx
Malachite	Mlc	$Cu_2(CO_3)(OH)_2$	x
Muscovite/ Sericite	Ms	$KAl_2((OH,F)_2\|AlSi_3O_{10})$	xx
Quartz	Qz	SiO_2	xxx
Rutile	Rt	TiO_2	xx
Serpentine	Srp	$(Mg)_3(Si_2O_5)(OH)_4$	x
Titanite (sphene)	Ttn	$CaTi(O\|SiO_4)$	x

x very rare to rare, xx common, xxx very common

[a] New defined abbreviation

[b] bb. covellite “Blaubleibender" covellite (mixture of spionkopite and yarrowite)

[c] due to replacement by Fe-(hydro)oxides

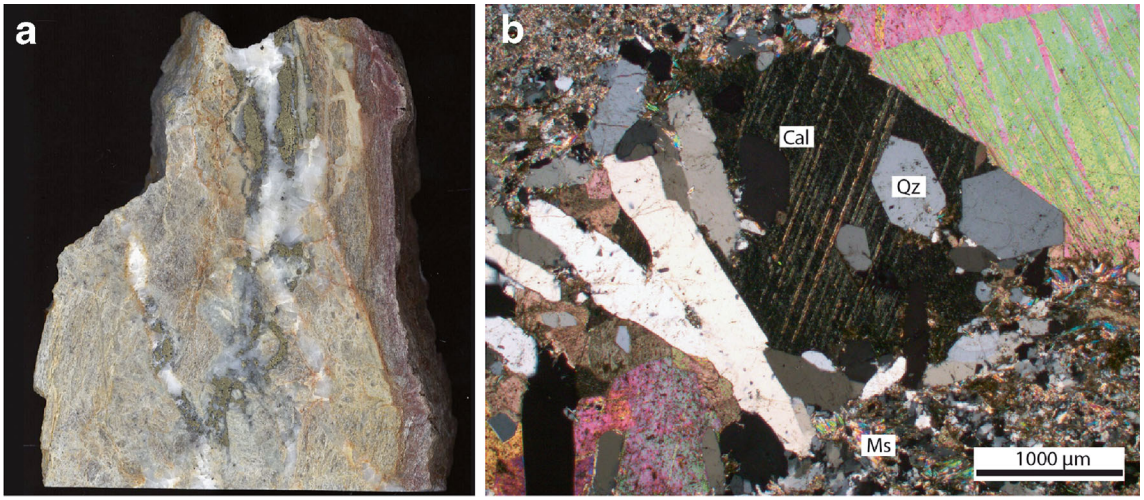

Fig. 4 **a** Ore sample (polished slab of sample T.03) from the Barbara dump, Weissenbach district. Carbonate-quartz-sulfide veinlets crosscut strongly altered host rock. Sample height ~10 cm. **b** Microphotograph showing veinlet with coarse calcite (Cc) and euhedral quartz (Qz) crosscutting altered gneissose host rock (*top left* and *bottom right*). Sericite (Mu) and carbonate are the common alteration minerals. Sample T.03, thin section, transmitted light, crossed-polars

observed in this specific sample; gold value of the bulk sample is also low (i.e., 3.5 ppm). Quartz is intergrown with calcite and the sulfides and partly forms perfectly euhedral crystals (Fig. 4b). The co-existing coarse-grained vein carbonate is calcite. Euhedral rutile was also observed in the veinlet.

The altered host rock around the veinlets contains sericite, calcite and quartz (Fig. 4a, b). Rutile and other Ti-minerals (titanite, anatase?) likely also belong to the alteration assemblage. From the primary host rock mineralogy only quartz, and to some extent, muscovite, are preserved; no feldspars are present any more. Locally, muscovite may define a ghost-like relict foliation. Thus, sample T.03 represents sericite-carbonate alteration that affected a siliceous quartz-mica-(feldspar?)-rich rock. Most likely the unaltered protolith was a biotite-muscovite-bearing paragneiss from the amphibolite-biotite gneiss unit.

Paragenetic stages—an overview

Based on ore microscopy and EMPA analyses three paragenetic stages can be distinguished (Fig. 5). This figure provides only a summary; the detailed mineralogy of each sample is listed in electronic supplementary material appendix 2. The minerals identified, nominal mineral compositions together with mineral abbreviations are given in Table 1.

Stage 1 includes the earliest formed Cu-Fe-As sulfides, which were replaced by the younger stage 2 and 3 assemblages. The main ore minerals of this stage are chalcopyrite, pyrite and arsenopyrite. Associated minor minerals include alloclasite, sphalerite, galena, bismuth and matildite. Gold was observed in several samples of this stage. The associated gangue minerals are quartz and calcite.

Stage 2 includes the Cu-(Fe)-sulfides and Cu arsenides that formed by replacement of stage 1 sulfides. It includes bornite, enargite and various minerals of the Cu-S and Cu-As system. The most common Cu-S phases are chalcocite/digenite, anilite and bb covellite (bb "blaubleibend"=German for blue remaining), others like djurleite, geerite etc. are more rare (Table 1). The most common Cu-arsenide is domeykite; it occurs together with minor koutekite. Gold is also associated with this

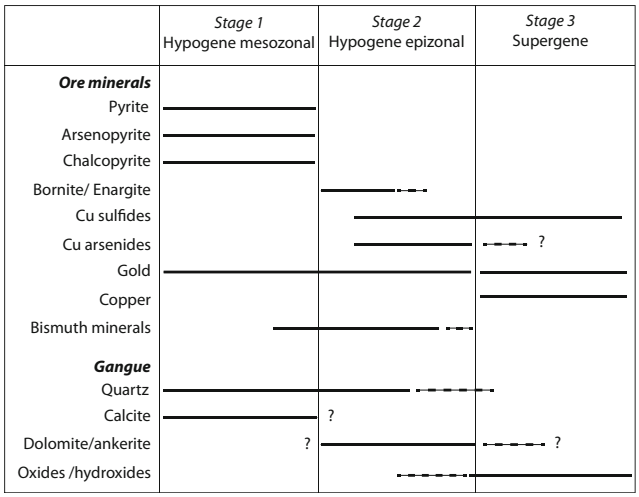

Fig. 5 Paragenetic stages distinguished in vein-type Cu-Au mineralization in the Flatschach mining area. Gold is present in all three stages. Cu-rich sulfides include digenite, djurleite, anilite, geerite, spionkopite and yarrowite; Cu-rich arsenides are domeykite, koutekite and enargite; bismuth phases include bismuth, bismuthinite and matildite (see text for details). *Solid line*: common, *dashed line*: less common phase

stage. The common gangue minerals are dolomite/ankerite and quartz.

Stage 3 includes oxides, hydroxides and copper carbonates that formed during supergene weathering. These are hematite, cuprite, goethite, malachite and azurite. The Cu sulfides anilite, djurleite, bb covellite as well as copper could also be low-T phases related to supergene oxidation/cementation processes. Their assignment to stage 2 vs stage 3 is sometimes uncertain. Gold of finer grain size (max. 20 μm) and different chemical composition is also part of this stage.

Arsenopyrite, pyrite and chalcopyrite

Chalcopyrite, pyrite and arsenopyrite are the most frequent ore minerals in stage 1 (Fig. 5, electronic supplementary material appendix 2). Arsenopyrite and pyrite show sub- to euhedral morphology (Fig. 6a, b). Two generations of pyrite can be distinguished. The first generation (Pyrite I) is inclusion-free, euhedral and intergrown with arsenopyrite. The second generation (Pyrite II) is finer grained, inclusion-rich and intimately intergrown with the gangue minerals; partly it overgrows Pyrite I and arsenopyrite (Fig. 6a). The larger pyrite and arsenopyrite grains often show cataclastic texture. Chalcopyrite fills fractured pyrite and arsenopyrite (Fig. 6b) but it also occurs as large anhedral (±fractured) grains, commonly with inclusions of euhedral pyrite and arsenopyrite, or disseminated in carbonate gangue. Locally, chalcopyrite overgrew euhedral gangue quartz.

In stages 2 and 3 chalcopyrite, pyrite and arsenopyrite occur only as relicts that were incompletely replaced by bornite and various Cu sulfides and Cu arsenides. Bornite forms coronas around chalcopyrite or is present in micro-fractures and oriented lensoid lamellae within chaclopyrite. Some of the coronas are poly-phase and include, in addition to bornite, digenite and bb covellite (Fig. 6d). Pyrite and chalcopyrite are commonly altered to Cu-rich sulfides (e.g., digenite, anilite etc.; Fig. 7a). In the oxidized stage 3, chalcopyrite is exclusively preserved as tiny rounded inclusion in euhedral quartz (Fig. 7d).

Chemical compositions of arsenopyrite, pyrite and chalcopyrite are listed in Table 2. Some pyrites contain minor arsenic (up to 2.1 mass % As, J03 an1), others not (sample 78568) confirming that there are chemically different types of pyrite. Compositions of chalcopyrite are close to ideal $CuFeS_2$. In contrast arsenopyrite composition is non-ideal; it contains excess sulfur (1.09–1.15 S per formula unit; Table 2).

Cu-rich sulfides and copper

Cu-rich sulfides observed include digenite/chalcocite, anilite, djurleite and bb covellite (Tables 3, 4); actually, the latter is now known to be a mixture of spionkopite $Cu_{1.39}S$ and yarrowite $Cu_{1.13}S$ (Goble 1980). The identification of these minerals is based on optical properties observed in reflected light in combination with EMPA analyses.

The Cu-sulfides commonly exhibit replacement and cataclastic textures; i.e., the larger grains are often fractured and fragmented, the micro-fractues being filled with gangue minerals. Chalcocite/digenite and anilite mainly formed by replacement of chalcopyrite, bornite and pyrite (Figs. 6d, 7a). Fine-grained covellite also occurs in cloud-shaped micro-areas together with bismuth. In sections with a higher

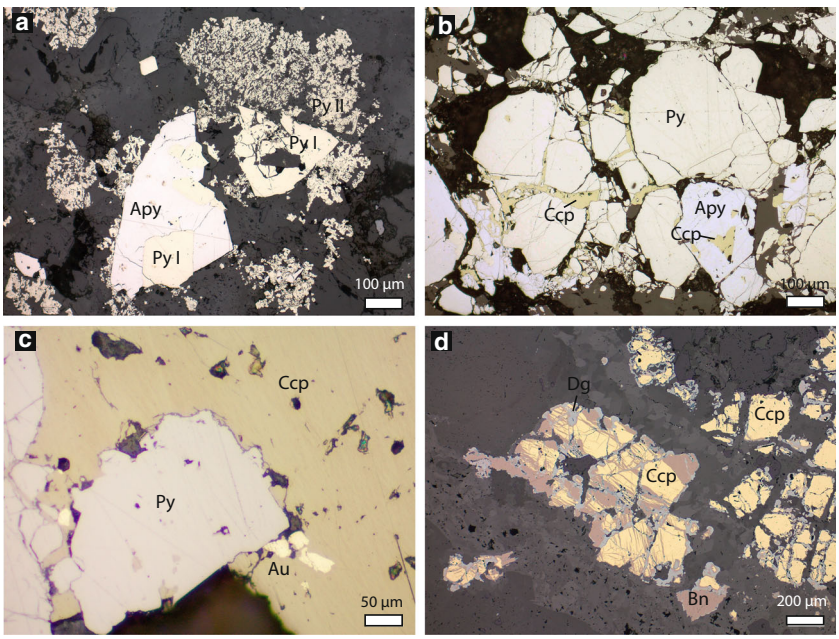

Fig. 6 **a** Two generations of pyrite (Py I and Py II) and arsenopyrite (Apy) in quartz calcite gangue. Stage 1. Sample 78561. **b** Chalcopyrite (Ccp) filling fractured pyrite (Py). Minor arsenopyrite (Apy) is also present. Stage 1. Sample J.05. **c** Stage 1 pyrite (Py), chalcopyrite (Ccp) and gold (Au). Stage 1. **d** Chalcopyrite (Ccp) replaced by bornite (Bn), digenite (Dg) and bb covellite. Transition of stage 1 to stage 2. Sample 78568

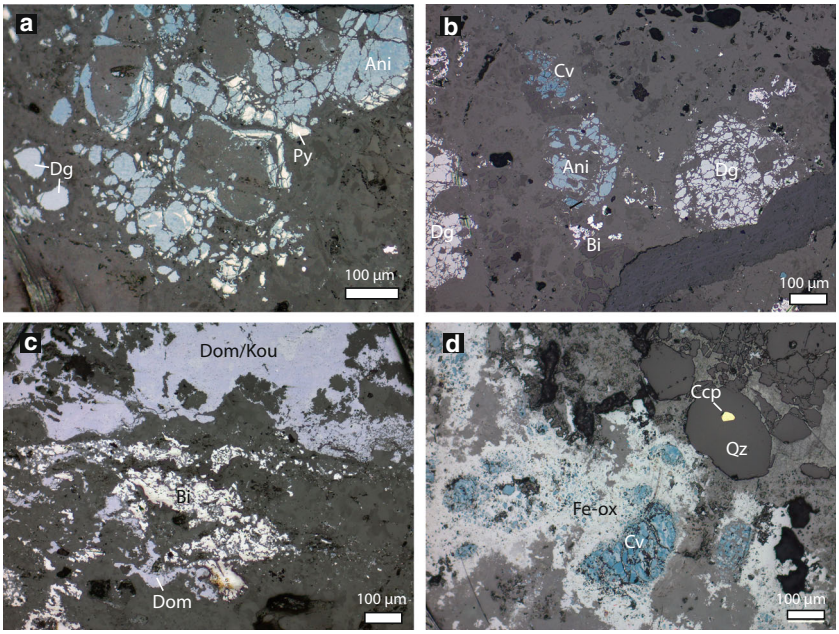

Fig. 7 **a** Digenite (Dg) and anilite (Ani) formed by replacement of pyrite (Py). Sample P.12. **b** Digenite, anilite (Ani) and bb covellite (Cv) with bismuth (Bi). Note the increase in blue hue in these phases. Stage 2. Sample P.7. **c** Domeykite / koutekite (Dom/Kou) intergrown with bismuth (Bi) in carbonate gangue. Stage 2. Sample P.18, few days after re-polishing. **d** Mixture of hematite /Fe-hydroxide (Fe-ox) replacing bb covellite (Cv). Chalcopyrite (Ccp) of stage 1 is only preserved as inclusion in quartz (Qz). Stage 3. Sample P.22

amount of bismuth (e.g., P.15), digenite is intergrown with this phase. In sections with a high amount of oxide/hydroxide gangue (stage 3), digenite is mainly absent and covellite becomes the dominant Cu-sulfide (Fig. 7d). Bb covellite is locally intergrown with copper. Larger (>100 μm) grains of copper show skeletal / dendritic morphology but it is also present as fine disseminated dust in calcite that is replaced by Fe-oxide/hydroxide (stage 3). There, copper is partly oxidized to cuprite.

Analyses of minerals of the Cu-S system are listed in Tables 3 and 4. Discrimination of these phases is mainly based on their different Cu/S ratio (e.g., Posfai and Buseck 1994) but also considering optical properties. Digenite has compositions of $Cu_{1.88–1.99}S$. Chemically analyses close to Cu_2S (e.g., P12 an10, Table 3) could, however, also be chalcocite. Similarly, identification of djurleite on basis of chemical composition is equivocal. Anilite has Cu/S of about $Cu_{1.71–1.82}S$. Bb covellite is according to its chemcial composition yarrowite ($Cu_{1.14–1.18}S$) as well as spionkopite ($Cu_{1.38–1.39}S$). It must be noted that structural data supporting unequivocal identification of these phases is not available.

Domeykite, koutekite, enargite and safflorite

Domeykite and koutekite are quite common phases in the Weissenbach district (Brandnergang) and less common elsewhere (electronic supplementary material appendix 2). These copper arsenides form irregular aggregates of different shape and are commonly associated with carbonate gangue of stage 2. They form irregular patches (Fig. 7c) but also occur in a reticulate network of micro-fractures and as irregular "reef-like" aggregates (Fig. 8d) where these phases are porous. In some samples, domeykite/koutekite are associated with bismuth, digenite and gold (Figs. 7c, 8e).

Regarding their Cu/As ratio a *continuous* compositional variation is evidenced in the domeykite—koutekite data (Table 5). The Cu/As ratios vary between 2.5 and 2.8 but never reach up to 3. Thus, according to its chemical composition domeykite is rather β-domeykite than α-domeykite (Cu_3As). Analyses with Cu/As of 2.5–2.6 are classified as koutekite (Table 5). Analyses of both domeykite and koutekite may contain small but erratic amounts of Fe (0.02 to 3 mass%). Thus Fe is rather a contaminant than incorporated in the structure.

Enargite is a rare phase formed during replacement of stage 1 chalcopyrite and arsenopyrite. It was observed in reaction coronas around chalcopyrite together with tetrahedite (?). One enargite analysis is listed in Table 5. Safflorite was only observed in sample 78566, where it is associated with chalcopyrite. Tiny euhedral to subhedral safflorite crystals form elongate aggregates or star-shaped groups.

Bismuth minerals

The bismuth minerals in the samples include mainly bismuth and rare bismuthinite and matildite. Bismuth mainly occurs in carbonate and oxides/hydroxide gangue, either finely disseminated or in larger (up to 1 × 6 mm) irregular patches. It is quite common in stage 2 where it is associated with digenite, anilite and domeykite/koutekite (Fig. 7b, c). In a few cases has it been observed together with gold, matildite and bismuthinite associated with stage 1 chalcopyrite, pyrite and arsenopyrite. Bismuthinite is intergrown with or overgrowing bismuth; these polyphase grains are usually small (<10 μm). Elongated

Table 2 Chemical composition of pyrite, chalcopyrite and arsenopyrite determined by EMPA

	Arsenopyrite								Pyrite				Chalocpyrite			
	78568 an9	78568 an11	P18 an2_38	J03 an2_64	J03 an2_69	J03 an2_72	J03 an2	P1 an10	78568 an2	J03 an1	J03 an3	J05 an3	J05 an2	78568 an8	78568 an12	J03 an4
m.%																
Cu	bld	bld	0.26	0.02	bld	bld	bld	0.18	0.011	bld	bld	bld	34.62	34.43	34.58	34.52
Fe	36.80	36.69	36.91	36.89	36.78	36.94	36.26	35.92	47.22	46.63	46.98	46.82	30.71	30.87	30.75	30.88
As	39.31	40.38	39.22	39.45	39.77	40.17	40.77	42.50	bld	2.08	1.54	1.78	0.01	bld	bld	0.04
S	24.68	23.72	22.26	22.28	22.27	21.95	23.26	22.05	53.59	51.97	51.86	52.46	34.73	34.92	35.15	34.66
Sum	100.81	100.79	98.65	98.64	98.82	99.07	100.32	100.65	100.82	100.68	100.38	101.06	100.07	100.22	100.48	100.10
at.%																
Cu	0.00	0.00	0.22	0.00	0.00	0.00	0.00	0.15	0.01	0.00	0.00	0.00	25.04	24.84	24.86	24.97
Fe	33.73	33.94	35.10	35.09	34.96	35.14	33.83	33.83	33.59	33.62	33.93	33.56	25.24	25.30	25.12	25.38
As	26.85	27.84	27.80	27.97	28.17	28.48	28.35	29.84	0.00	1.12	0.83	0.95	0.00	0.00	0.00	0.02
S	39.40	38.22	36.88	36.92	36.87	36.37	37.80	36.18	66.40	65.27	65.24	65.49	49.72	49.86	50.02	49.62
Sum	100	100	100	100	100	100	100	100	100	100	100	100	100	100	100	100
Fe+As+S=3													Fe+Cu+As+S=4			
Cu	0.001	0.000	0.007	0.001	0.000	0.000	0.001	0.004	0.000	0.000	0.000	0.000	1.002	0.993	0.994	0.999
Fe	1.012	1.018	1.053	1.053	1.049	1.054	1.015	1.015	1.008	1.009	1.018	1.007	1.010	1.012	1.005	1.015
As	0.806	0.835	0.834	0.839	0.845	0.854	0.851	0.895	0.000	0.034	0.025	0.029	0.000	0.000	0.000	0.001
S	1.182	1.147	1.106	1.108	1.106	1.091	1.134	1.085	1.992	1.958	1.957	1.965	1.989	1.994	2.001	1.985
Sum	3	3	3	3	3	3	3	3	3	3	3	3	4	4	4	4

bld below limit of detection

Table 3 Chemical composition of digenite/ chalcocite determined by EMPA

Mass%	P7an3	P7an9	P7an23	P12an10	P12an11	P12an20	P1an3	P1an5	P1an9	P10an1	P10an2	P10an3
Cu	79.65	79.63	79.24	79.72	80.08	79.76	80.15	80.32	79.87	80.10	79.64	79.61
Fe	0.12	0.18	0.33	0.55	0.39	0.28	0.00	0.00	0.00	0.05	0.03	0.44
As	bld	bld	0.16	bld	bld	0.13	bld	bld	bld	bld	bld	bld
S	20.93	20.77	21.24	20.26	20.36	20.45	20.35	20.49	20.49	20.36	20.58	20.59
Total	100.70	100.58	100.97	100.53	100.83	100.61	100.50	100.81	100.36	100.51	100.25	100.64
Atoms per S=1												
Cu	1.921	1.935	1.882	1.986	1.985	1.968	1.987	1.978	1.967	1.985	1.953	1.951
Fe	0.003	0.005	0.009	0.016	0.011	0.008	0.000	0.000	0.000	0.001	0.001	0.012
As	0.000	0.000	0.003	0.000	0.000	0.003	0.000	0.000	0.000	0.000	0.000	0.000
S	1.000	1.000	1.000	1.000	1.000	1.000	1.000	1.000	1.000	1.000	1.000	1.000
Cu/S	1.92	1.93	1.88	1.99	1.98	1.97	1.99	1.98	1.97	1.99	1.95	1.95

bld below limit of detection

grains of bismuth/bismuthinite up to 10 mm in size were found in drill cores rich in chalcopyrite during the exploration campaign of Noricum Gold Limited in 2014 in the Brunngraben district; they are associated with gold (Paar 2014). Matildite also occurs in approximately 20 μm polymineralic grains intergrown with bismuth.

Analyses of bismuth minerals are listed in Table 6. The analyses of bismuth are commonly close to 100 mass%. Minor concentrations of Cu or Fe likely are due to matrix effects. Bismuthinite is rather pure Bi_2S_3; it only contains small amounts of Cu, Fe, ±Sb. Matildite is a main carrier of silver (24.5–25.5 mass% Ag) and may contain minor Cu. One analysis of matildite yielded 3.7 mass% of Sb.

Gold

Gold has been documented in all three paragenetic stages (Fig. 5; electronic supplementary material appendices 1 to 3). Stage 1 gold occurs along the grain boundaries between chalcopyrite and arsenopyrite (Fig. 8a, c) and in fractures in gangue. In some cases, gold occurs in clusters of grains of very variable grain size. The shapes are commonly irregular. Gold in this stage shows composition of Au/Ag from nearly pure gold to electrum.

Subrounded to angular shaped gold in stage 2 occurs primarily in carbonate gangue together with digenite (containing relicts of pyrite), domeykite/koutekite and bismuth (Fig. 8d). In only a few cases it occurs in contact with Cu-rich sulfides such as digenite (Fig. 8e).

In stage 3, gold mainly occurs in patchy clusters to linear arrays consisting of multiple small grains embedded in the oxide/hydroxide matrix, including hematite (Fig. 8f). In sample P22, gradual replacement of Cu-sulfides can be observed. In a first step digenite and anilite are transformed to bb covellite and subsequently the Cu sulfides are replaced by the Fe-oxide/hydroxide assemblage (Fig. 8f).

The sizes of gold grains have been measured because of their relevance to ore recovery techniques. The grain

Table 4 Chemical composition of anilite and covellite (yarrowite, spionkopite) determined by EMPA

Comment Mass%	P7an4 Ani	P12an13 Ani	P12an14 Ani	P1an6 Ani	P1an8 Ani	P7an6 Cv / Yar	P7an7 Cv / Spk	P12an9 Cv / Yar	P12an17 Cv / Yar	P12an21 Cv / Yar	P1an12 Cv / Spk	P1an14 Cv / Yar
Cu	77.91	78.19	78.06	78.14	77.79	69.18	72.86	69.95	69.21	68.78	73.33	69.19
Fe	0.39	0.49	0.60	0.02	0.13	1.97	1.96	0.58	0.98	1.02	0.31	0.57
As	bld	bld	bld	bld	bld	bld	bld	bld	bld	0.37	bld	bld
S	21.55	22.36	22.30	22.19	22.58	29.67	26.72	30.68	30.59	29.68	26.56	30.54
Total	99.85	101.04	100.96	100.38	100.50	100.82	101.54	101.21	100.78	99.85	100.20	100.30
Atoms per S=1												
Cu	1.824	1.765	1.766	1.777	1.738	1.176	1.376	1.150	1.142	1.169	1.393	1.143
Fe	0.010	0.013	0.016	0.000	0.003	0.038	0.042	0.011	0.018	0.020	0.007	0.011
As	0.000	0.000	0.000	0.001	0.000	0.000	0.000	0.000	0.000	0.005	0.000	0.000
S	1.000	1.000	1.000	1.000	1.000	1.000	1.000	1.000	1.000	1.000	1.000	1.000
Cu/S	1.82	1.76	1.77	1.78	1.74	1.18	1.38	1.15	1.14	1.17	1.39	1.14

bld below limit of detection

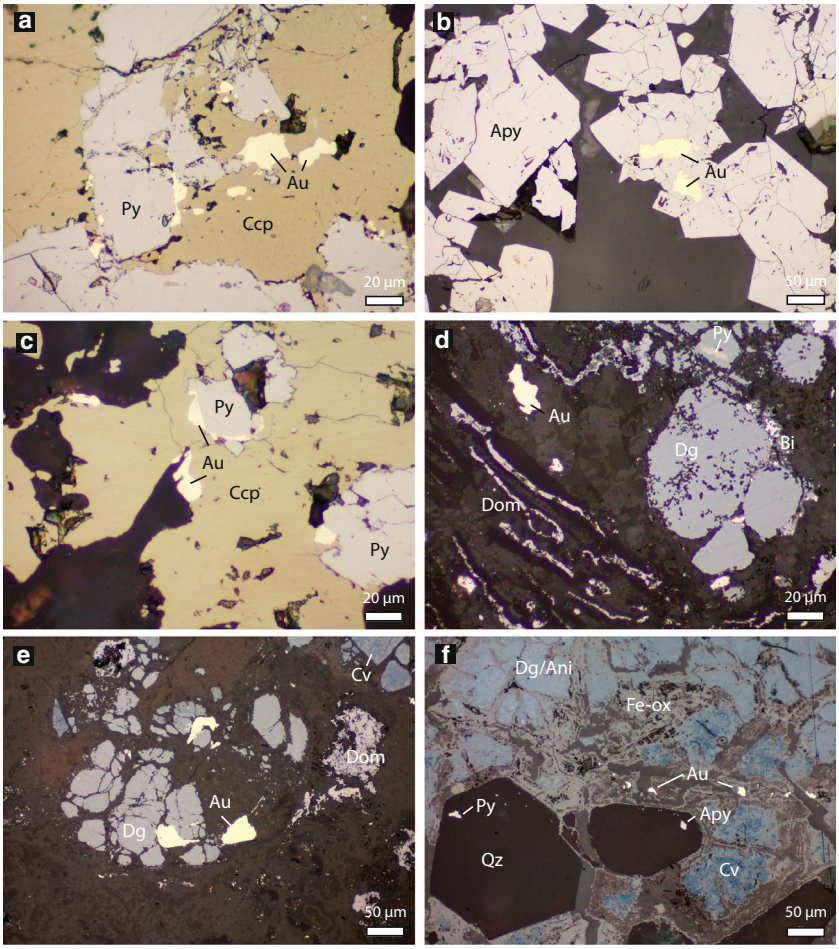

Fig. 8 Gold in the paragenetic stages 1 to 3. **a**–**c** Gold associated with chalcopyrite (Ccp), pyrite (Py) and arsenopyrite (Apy). Stage 1. Samples 78568 (**a**, **c**) and J.05 (**b**). **d** Gold and bismuth (Bi) in Ca-Mg-Fe-carbonate gangue together with digenite (Dg, containing relicts of pyrite (Py)) and reef-like stringers of domeykite (Dom). Stage 2. Sample P.10. **e** Gold associated with digenite (Dg), bb covellite (Cv) and domeykite (Dom). Stage 2. Sample p.07. **f** Cluster of small gold grains (Au, high reflectance) in fractured matrix of oxides/hydroxides (Fe-ox). Bb covellite (Cv) forming pseudomorphs after digenite/anilite (Dg/Ani) and is itself replaced by the Fe-oxide/hydroxide (Fe-ox) assemblage. Euhedral quartz (Qz) contains inclusions of pyrite (Py) and arsenopyrite (Apy). Stage 3. Sample P.22

size distribution of gold is illustrated in boxplots (Fig. 9). The median grain size of stage 1 gold is 5 µm with a large number of grains plotting as outliers outside the box toward larger grain sizes. Gold from stage 2 seems to be slightly coarser-grained (median= 14 µm) but with a larger uncertainty. There is a considerable overlap with stage 1. The grain size of stage 3 gold (median=5 µm) is comparable to stage 1 but larger gold grains are missing. Hence, gold grains >20 µm are restricted to stages 1 and 2.

Table 5 Chemical composition of domeykite, koutekite and enargite determined by EMPA

Mass%	P7an2_22 Kou	78568an2_27 Kou	P18an2_40 Dom	P18an2_41 Dom	P18an2_46 Dom	P18an2_48 Dom	P18an2_49 Kou	P12an2_54 Dom	P12an2_55 Dom	P12an2_62 Dom	J03-10 Eng
Cu	67.26	66.16	70.69	69.84	68.49	69.79	67.59	68.74	68.83	70.56	48.34
Fe	0.92	3.02	bld	0.17	0.67	bld	0.15	1.53	1.94	0.72	0.15
As	31.57	30.23	29.44	30.53	31.01	29.49	32.13	30.48	29.70	30.02	17.31
S	bld	bld	bld	0.05	bld	bld	0.13	bld	0.10	bld	33.45
Total	99.76	99.43	100.17	100.59	100.17	99.30	100.00	100.75	100.57	101.30	99.25
Atoms per As=1											S=4
Cu	2.515	2.584	2.835	2.701	2.608	2.794	2.484	2.663	2.736	2.775	2.916
Fe	0.039	0.134	0.000	0.007	0.029	0.000	0.006	0.067	0.088	0.032	0.01
As	1	1	1	1	1	1	1	1	1	1	0.886
S	0.000	0.000	0.000	0.004	0.000	0.000	0.010	0.000	0.008	0.000	4
Cu/As	2.52	2.58	2.84	2.70	2.61	2.79	2.48	2.66	2.74	2.78	3.29

bld below limit of detection

Table 6 Chemical composition of bismuth, bismuthinite and matildite determined by EMPA

Sample/Spot no. Mass(%)	P18 sulfo-20 Bismuth	78568 sulfo-2 Bismuth	78568 sulfo-6 Bismuthinite	78571 sulfo-11 Bismuthinite	78568 sulfo-1 Matildite	78571 sulfo-16 Matildite
Fe	0.32	0.13	0.47	0.29	0.29	0.94
Sb	bld	bld	bld	0.39	3.69	bld
Cu	1.19	0.07	0.98	0.80	4.46	2.11
Ag	bld	0.33	0.08	0.20	24.52	25.54
Bi	97.96	97.01	80.46	79.77	47.64	54.79
S	bld	0.10	19.50	19.97	18.60	17.73
Total	99.47	97.66	101.64	101.42	99.20	101.11
Ions calculated on the basis of bismuthinite S=3, matildite S=2						
Fe	0.011	0.005	0.041	0.025	0.018	0.061
Sb	–	–	–	0.015	0.104	–
Cu	0.038	0.002	0.076	0.061	0.242	0.120
Ag	0.000	0.007	0.004	0.009	0.784	0.856
Bi	0.951	0.979	1.899	1.838	0.786	0.948
Sum Cations	1.000	0.993	2.020	1.948	1.934	1.985
S	–	0.007	3	3	2	2

Pb is always below the limit of detection (bld)

Gold was analyzed in 12 samples. A few representative analyses are listed in Table 7. The whole data set of gold analyses is put in a data repository (electronic supplementary material appendix 3) and graphically shown in a histogram (Fig. 10). Composition of gold in the three ore stages is illustrated in Au-Ag-Hg triangular plots (Fig. 11).

According to composition three populations are distinguished in the histogram showing gold fineness (Fig. 10). The dominant population has fineness of 640–860 (mean=725; n=46) and is classified as electrum. Pure gold with fineness 930–940 (n=6) is rare. Gold in the oxidized stage 3 is very Ag-rich electrum with fineness 350–490 (mean=412, n=12). In stages 1 and 2 the composition of gold is comparable, although stage 1 gold exhibits wider compositional variation with respect to Au/Ag (Fig. 11a, b; Table 7). Gold mainly differs in its Au/Ag but concentrations of Hg in gold of stage 1 may reach up to 14.3 mass%. Gold from the oxidized stage 3 sample P22 is commonly very rich in Hg (Fig. 11c).

Element mapping revealed that even on the micro-scale there exist two generations of gold. Gold-rich cores are surrounded by thin Ag-rich rims (Fig. 12).

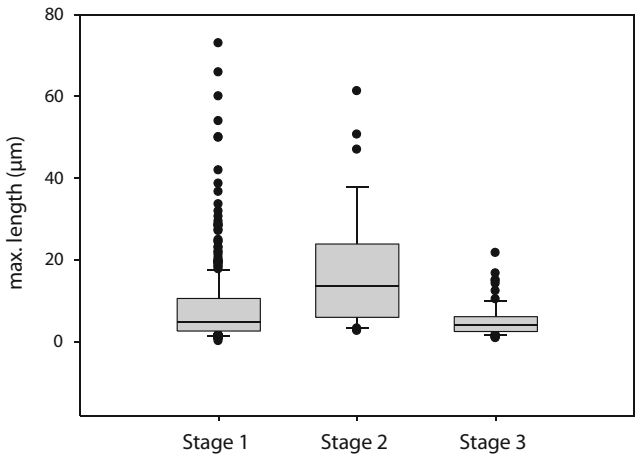

Fig. 9 *Box plot* showing distribution of grain size of gold in the three paragenetic stages; length refers to the maximum measurable distance of a grain in polished section or SEM image. *Horizontal line* in the *grey box* gives median value, lower and upper limit of *grey box* shows single standard deviation, error bars on *vertical line* give the lower and upper quartile values; outliers are shown as *black points*

Discussion

Mineralogical constraints on formation conditions

Stage 1

Some estimates about formation temperatures during the first and second mineralization stage can be deduced from mineralogy. The main ore minerals of stage 1 are arsenopyrite, pyrite and chalcopyrite. Associated minerals include enargite, sphalerite, galena, bornite, alloclasite, bismuth, matildite and gold.

The melting point of bismuth is ~269 °C and decreases with increasing pressure. Bismuth crystallizing from a melt phase is characterized by drop-shaped morphology and, when included in other sulfides, by concentric radial micro-fracture patterns (Ramdohr 1975). Such ore textures were, however, not observed; bismuth in the samples studied exclusively occurs in the carbonate gangue (formed after quartz) and not in

Table 7 Representative analyses (mass %) of gold determined by EMPA; the complete data set is available as electronic supplementary material appendix 3

Sample/ Spot no.	P.7 KR4-1	P.7 KR3-2	P.10 KR3-1	P.12 KR2-1	P.15 KR5-1	P.15 KR6-1	P.18 KA2	P.22 KR4-cl2
Au	93.52	77.33	73.45	73.45	93.38	67.09	73.30	47.00
Ag	5.92	20.74	23.86	23.25	5.75	31.54	23.81	38.67
Hg	0.45	2.55	2.41	2.27	0.57	1.12	2.63	10.18
Cu	0.48	0.04	0.55	0.05	0.13	0.62	0.17	0.70
Total	100.37	100.66	100.27	99.02	99.83	100.37	99.91	96,55[a]
Sample/ Spot no.	78562-1	78562-2	78568-1	78573-6	J.04-1	J.04-3	J.05-4	J.05-11
Au	76.5	95.22	64.13	76.75	40.55	64.1	72.38	69.3
Ag	20.48	5.48	30.84	21.73	39.02	28.07	23.28	26.61
Hg	3.4	0.26	3.88	2.01	14.29	7.72	3.79	3.9
Cu	0.07	0.06	1.03	bld	1.66	0.14	0.57	0.05
Total	100.45	101.01	99.88	100.49	95,52[a]	100.03	100.02	99.86

bld below limit of detection

[a] low total due to very small size of analysed grain

direct contact with other sulfides. It is therefore concluded that bismuth did not crystallize from a melt phase but formed as a solid below the melting point.

Matildite in the studied samples is very rare and small in size (<10 μm), which makes it difficult to determine whether the α-or β-modification is present. However, the backscattered electron images show neither exsolution of galena, nor kamacite-like internal texture, features, which would be typical for the transformation of α- to β-matildite (Ramdohr 1975). This suggests that α-matildite is the modification present in the studied material and that formation temperatures of matildite plus the associated gold in Stage 1 were >195 °C.

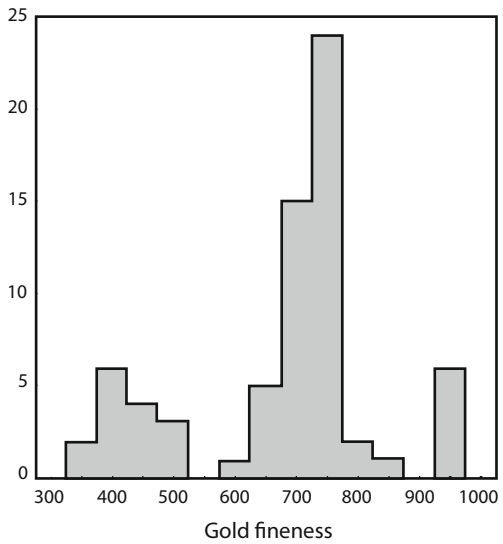

Fig. 10 Histogram showing the fineness of gold (n=69); fineness is parts of Au per 1000 (on mass% basis)

Arsenopyrite coexists with pyrite±chalcopyrite (without pyrrhotite) in the samples studied. The composition of arsenopyrite in the Fe-As-S system is temperature dependent and has been used as a geothermometer (Barton 1973, Kretschmar and Scott 1976, Sharp et al. 1985). Analyzed arsenopyrite contains 25.8 to 28.6 at.% of As (average 27.6±0.9); i.e., it is S-rich arsenopyrite. Exact temperatures were not calculated because we are not dealing with a univariant reaction (no pyrrhotite; Cu as additional component) and experimental data are not available for temperatures below 300 °C. From extrapolations of phase diagrams that were constructed for temperatures >300 °C (e.g., see Fig. 9 in Morey et al. 2008) it is, however, indicated that the arsenopyrite-pyrite assemblage at Flatschach formed at temperatures well below 300 °C.

We conclude that stage 1 assemblage is constrained between about ~200 and ~270 °C, which would fall in the lower temperature range of mesozonal gold deposits (Kerrich et al. 2000). Fluid inclusion data (not yet available) would be necessary for better constraining the P-T-X conditions of Cu-Au mineralization.

Stage 2

Stage 1 sulfides are to a variable extent replaced by the younger stage 2 Cu sulfides; e.g., replacement of chalcopyrite by bornite, digenite etc. The main ore minerals in stage 2 are the Cu sulfides digenite, anilite and yarrowite and the Cu-arsenides domeykite and koutekite. The dominant gangue minerals of stage 2 are Ca-Mg-Fe carbonates; quartz becomes less important. During the transformation of stage 1 to stage 2 assemblages iron, which was fixed in the sulfides pyrite, chalcopyrite and arsenopyrite, becomes oxidized and is

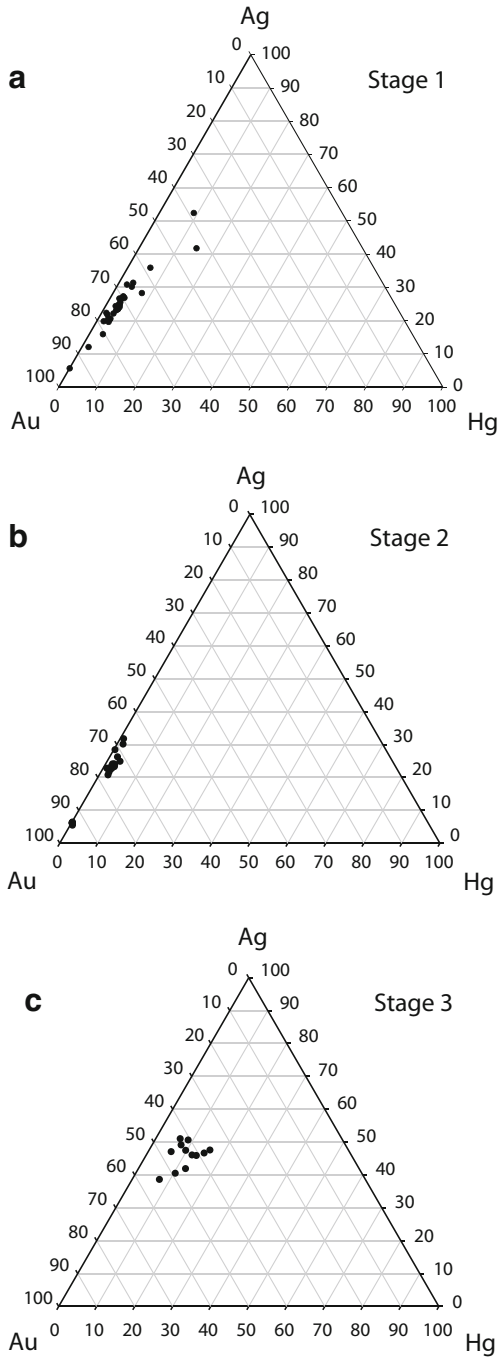

Fig. 11 **a**–**c** Chemical composition of gold shown in Au-Ag-Hg triangular plots (mole%) for the three paragenetic stages

incorporated in the gangue minerals; i.e., Fe-bearing carbonates, Fe-oxides/hydroxides.

The formation of the Fe-poor Cu-sulfide and Cu-arsenide assemblages of stage 2 could either be the result of a low-temperature hydrothermal overprint by ascending fluids *and/or* related to cementation during supergene weathering. The latter explanation was preferred by Paar and Meixner (1979) who observed optically isotropic α-domeykite in their material, which is only stable below 90±10 °C (Skinner and Luce 1971). However, transformation of α- to anisotropic β-domeykite, which is stable to higher temperatures, was also reported (Paar and Meixner 1979).

Some further constraints can be deduced from the phase relationships in the Cu-S system (see Fig. 12 in Barton 1973). According to this author bb covellite is only stable below 157 °C. The low-temperature limit of digenite+bb covellite is given at 76 °C, whereas anilite and bb covellite coexist <76 °C. At higher Cu/S ratio djurleite+anilite are stable at temperature below ~70 °C. Hence, the observed assemblage digenite+bb covellite constrain the temperature between 76 °C and 157 °C. Anilite+bb covellite were also observed as coexisting phases and djurleite, which was reported previously (Paar and Meixner 1979), was also confirmed in some samples in this study. According to Barton (1973) the maximum formation temperature of anilite- / djurleite-bearing assemblages is about 70 °C. A possible interpretation of this apparent discrepancy is that not *all* these phases are in equilibrium. The low temperature assemblages with anilite (± bb covellite), djurleite and α-domeykite could be related with cementation due to supergene weathering processes (stage 3). In contrast, the slightly higher-temperature assemblage digenite+bb covellite could still have formed during waning hydrothermal activity.

In summary stage 1 assemblage is comparable to mesozonal gold deposits (see below) but stage 2 is certainly of lower temperature. We may speculate that Flatschach represents a transitional meso- to epizonal copper-gold deposit.

Stage 3

Stage 3 comprises various oxides, hydroxides and carbonates of iron and copper, which formed during a late low-temperature oxidation event, in our interpretation during supergene weathering processes. Hematite, goethite, cuprite and malachite are the more commonly identified (by Laser Raman spectroscopy) phases in the studied material. Other secondary minerals reported from Flatschach area include aragonite and Cu-, Ni- carbonates, sulfates and arsenates, like annabergite, azurite, brochantite, devilline, erythrite, malachite, olivenite, posnjakite and tyrolite (mindat.org 2015).

The chemical changes of stage 3 are marked by a significant increase of ferric iron. Ferrous iron hosted in the primary stage 1 sulfides pyrite, chalcopyrite, and arsenopyrite is oxidized and fixed in Fe oxides and -hydroxides. The latter phases are often associated with copper, bb covellite (yarrowite), and rare anilite and djurleite.

Leaching experiments demonstrated that chalcocite and digenite are transformed through a series of metastable Cu sulfides, including anilite, bb covellite (geerite, spionkopite, yarrowite) to covellite and CuS_2 (Whiteside and Goble 1986).

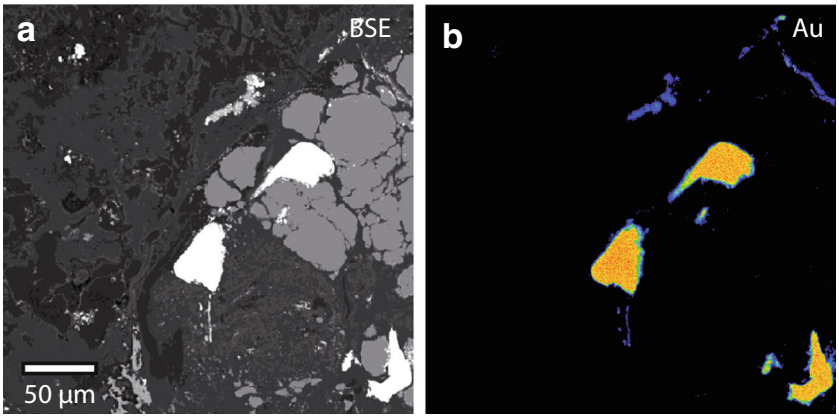

Fig. 12 Backscattered electron (**a**) and element mapping (**b**) of micro-area containing gold. Thin rims (*blue-green*) of gold grains (*yellow-red*) in (**b**) are lower in Au (and higher in Ag, not shown). Gold is associated with chalcopyrite and a Fe-rich carbonate phase. Sample P.7

Djurleite may form directly from digenite when affected by highly concentrated leachates (ferric sulfate $Fe_2(SO_4)_3 \cdot H_2O$).

These low-temperature Cu-sulfides and copper are therefore interpreted as the products of secondary enrichment by cementation due to weathering of the hydrothermal stage 1 and 2 sulfides and arsenides.

Interestingly, gold is still present in stage 3 assemblages. It is of finer grain-size compared to gold of stage 1 and 2, but its chemical composition overlaps. Actually, gold of stage 3 is quite rich in Ag and Hg. Because secondary (supergene) gold found in placers and regoliths is commonly very pure (e.g., Hough et al. 2009) it remains unclear if stage 3 gold is really newly formed and mobilized gold or relict gold preserved from the earlier hydrothermal stages.

Relationship of mineralization to regional metamorphism and tectonics

Copper-gold veins in the Flatschach area occur in various polymetamophic host rocks of the Austroalpine basement (Silvretta-Seckau nappe system). The host rocks are interpreted as the western continuation of metamorphic sequences in the Gleinalm area (Gaaler Schuppenzone, Schuster 2011). Amphibolites and plagioclase gneisses derived from mafic to intermediate volcanics, the intercalated biotite (±garnet±muscovite) gneisses and schists from siliciclastic sediments. Lenses of strongly serpentinized ultramafic rocks are correlated with the restitic mantle fragments of meta-ophiolites of the Late Proterozoic to Early Palaeozoic (?) Speik Complex. Other major lithologies include orthogneisses and granite gneisses. Due to the presence of coarse-grained feldspar porphyroclasts and of locally preserved intrusive contacts, the latter rocks are interpreted as metagranitoids intruding the older volcano-sedimentary unit. The emplacement age of these metagranitoids in the study area is unknown. Some of them could be equivalents of Variscan metagranitoids in the Seckau complex, for which Lower Carboniferous ages were reported (Frank et al. 1983; Scharbert 1981).

Regional metamorphism in the study area is poly-phase. Except the Mesozoic cover rocks (Rannach Formation) all other units experienced pre-Alpine as well as Eoalpine metamorphism (Faryad and Hoinkes 2003; Gaidies et al. 2006). The pre-Alpine metamorphic events include Permian low-pressure metamorphism (e.g., in the Koralpe Wölz nappe system, Schuster and Stüwe 2008) as well as a medium-pressure event of Upper Carboniferous age (Faryad and Hoinkes 2003) and an even older eclogite facies metamorphism (~400 Ma, Faryad et al. 2002). Late Cretaceous (~90–100 Ma Eoalpine metamorphism reached upper greenschist to amphibolite/eclogite facies conditions along a ~50 km long north–south transect (Faryad and Hoinkes 2003; Tenczer and Stuewe 2003) and is characterized by strong isothermal decompression. Mineral assemblages in metapelites (garnet+biotite+muscovite±kyanite) and metabasites (hornblende+plagioclase±garnet) indicate that peak conditions reached about lower amphibolite facies conditions in the study area. From the regional context and Ar-Ar cooling ages (Pfingstl et al. 2015) it is interpreted that peak assemblages are Eoalpine. Eoalpine high-pressure and subsequent medium-pressure Barrovian-type regional metamorphism is linked to subduction of the Meliata ocean and subsequent continent-continent collision between the European and Apulian plates in the late Cretaceous (Schmid et al. 2004)

The Cu-Au mineralization in the Flatschach area is strictly structurally controlled. It is bound to steep dipping NE-SW to NNE-SSW trending quartz-carbonate veins that formed in a brittle deformation regime. The veins are discordant and clearly crosscut the major lithological boundaries and the foliations and their formation post-dates the metamorphic peak assemblages. Hence, they can be classified as late to post-orogenic. Interestingly the historic mining sites in the Flatschach area are commonly located in areas where banded amphibolites predominate and are less well developed in zones where the host rock are gneisses. The mineralized veins show evidence of poly-phase brittle deformation. Cataclastic deformation of sulfides is observed in the polished sections; e.g., sulfide

Table 8 Comparison of Flatschach Cu-Au mineralization with features of orogenic and intrusion-related gold deposits. See footnote for sources

	Flatschach Cu-Au deposits	Orogenic gold deposits[1]	Intrusion-related gold deposits[2]
Geotectonic setting	Convergent plate margins: Mesozoic to Neogene collision of European with Adriatic plate	Convergent plate margins: complex orogenic belts, fore-arc region of convergent plate margins	Convergent plate margins: Cordilleran-type orogens; accretionary orogens; arc to collision deformed shelf sequences in accreted terranes
Host rocks and ore localisation	Amphibolite, biotite-plagioclase gneiss, orthogneiss, granite gneiss, minor serpentinite; pre-Variscan to Variscan age of protoliths (siliciclastic sedimentary rocks, mafic to felsic volcanics, granitoids)	Metabasites (sometimes meta-ultramafics), felsic igneous rocks, metamorphosed marine siliciclastic sedimentary rocks	Undeformed (!) small granitoid plutons, sills, dykes; cupolas and thermal aureoles around *reduced* post-arc (calc-alkaline to alkaline) granitoids (S-type); mineralization coeval with plutonism; sedimentary to metamorphosed siliciclastic rocks
Age of mineralization	Phanerozoic: Late Cretaceous to Neogene	Archaean to Phanerozoic, in Alps mostly Neogene (30–10 Ma)	Proterozoic (?) to mainly Phanerozoic
Structural control	NE-SW to NNE-SSW veins, local extensional veins related to late-stage regional compressional tectonics	2nd to 3rd order structures related to large-scale compressional crustal structures; late tectonic structures	Post-orogenic regional stress field may control orientation of veins
Type of mineralization	Steep veins/fracture zones, vertical or lateral zonation ?	Uniform mineralization style: veins, shear zones; little vertical zoning except Sb-Hg in epizonal parts	Variation of types and styles of mineralization: sheeted veins, stock-work, disseminated, breccia-hosted, skarns; zonal arrangement of veins: Au-As, Sb±Au-As; Ag-Pb-Zn; association with Sn, W deposits
Timing to peak metamorphism	Late to post-peak metamorphic	Syn- to post-peak metamorphic	Post-metamorphic
Depth of formation	Meso- to epizonal (?)	Considerable depth range: often mesozonal but epi- and hypozonal examples are known	Wide range, epi- to mesozonal (most deposits between 4 km and 6 km)
Element association	Cu, Au, Ag, As, Bi, (Hg, Co, Zn, Pb)	Au, Ag (±As, Sb, Te, W, Mo, Bi, B); minor Cu, Pb, Zn, Hg	Au-Bi-Te±W; Au-As±W±Sb; Au-As-Sb±Ag±Pb±Zn; significant Cu lacking!
Gold concentrations; Au:Ag ratio	Gold grades not available, Au:Ag (stage 1): 4-5	Au:Ag 10 (normal) to 1 (rare)	Low Au grade (<1 g/t Au); variable gold grade; good Au-Bi correlation
Ore mineralogy	Stage 1: Gold with chalcopyrite, pyrite, arsenopyrite Stage 2: Cu sulfides (digenite, anilite, etc.) and Cu arsenides (domeykite, koutekite)	Gold/electrum with pyrite, pyrrhotite, arsenopyrite etc. Sulfosalts, tellurides	Low fS_2 assemblages: pyrrhotite, arsenopyrite, pyrite; scheelite etc.
Gangue mineralogy	Quartz, calcite, dolomite/ankerite	Quartz±carbonates, ±albite, ±white mica, ±fuchsite, ±chlorite, ±scheelite, ±tourmaline	Quartz, feldspars low sulfide content (<1 vol.%)
Alteration	Sericite-carbonate-quartz	Sericitization, chloritization; quartz, Ca-Fe-Mg carbonates, sericite, albite, sulfides	Greisen alteration; Ksp-(biotite); albite-sericite; sericite-carbonate
Types of fluids	No data available	Aqueous-carbonic (>5 mol% CO_2), often immiscible; low salinity, small amounts of H_2S, CH_4, CO_2 and N_2	Aqueous-carbonic; low to high salinity CO_2-rich; ±CH_4; immiscible H_2O-NaCl brine and low saline H_2O±CO_2 in epizonal deposits
Pressure temperature (PT) conditions of ore formation	Stage 1: ~200–270 °C; P ? Stage 2: ~70–160 °C; P ?	220–500 °C, 0.05–0.4 GPa; many deposits 300±50 °C and 0.1 to 0.3 GPa	Wide PT range; often >350 °C; 0.03 to 0.35 GPa

Sources: [1] Groves et al. 1998, 2003; Kerrich et al. 2000; Goldfarb et al. 2005; [2] Hart and Goldfarb 2005

grains are tectonically rounded, micro-fractured and brecciated.

The exact age of vein formation and the Cu-Au mineralization is unknown although field relations allow bracketing the timing of ore formation. As argued above the veins must be post-peak metamorphic; i.e., younger than ~90 Ma. On the other hand they must be older than the transgressive coal-bearing strata of the Neogene Fohnsdorf basin because the latter overlay the ore veins at the Fortuna Unterbau addit (Jarlowsky 1951). Hence, the age of the Cu-Au-bearing structures is post-Late Cretaceous but pre-Early/Middle Miocene. It is not clear if stage 1 and stage 2 assemblages formed at about the same time during a continuous mineralization event (e.g., cooling of the system) or if stage 2 assemblages represent a separate much younger low temperature overprint.

The veins at Flatschach formed during the Alpine orogeny. This could have been in the cooling stage of Cretaceous regional metamorphism *and*/*or* even later during the Neogene. The Fohnsdorf basin to the south of the study area formed as a pull-apart basin in the Neogene and is related to the sinistral WSW-ENE Mur-Mürz strike-slip fault system (Fig. 1a, b). Theoretically, the mineralized NE-SW oriented veins could be small-scale structures related to this main fault system. However, as pointed out above the mineralized veins are of pre-Neogene age. Also the temperatures in the basin (max. ~70 °C, sub-bituminous coal) were likely too low for gold-transporting fluids. Thus, we prefer to link formation of the Cu-Au veins with late orogenic Eoalpine processes; i.e., transport of gold in metamorphic hydrothermal fluids, which focused in britte-semiductile structures developed during the cooling stage of Late Cretaceous metamorphism. Recognition of extension-related exhumation of the Seckau complex between 85 Ma and 80 Ma (Pfingstl et al. 2015) is in favor of this latter model.

Classification of Flatschach Cu-Au deposits

Features of Cu-Au deposits in the Flatschach area are compared to those of orogenic and intrusion-related gold deposits in Table 8. Similar to both classes of gold deposits Cu-Au veins at Flatschach developed at destructive plate margins during orogenic collision; i.e., during the Alpine orogeny in the late Mesozoic to Neogene when the (upper) Adriatic plate collided with the (lower) European plate (Schmid et al. 2004).

In contrast to intrusion-related gold deposits at Flatschach there is no immediate spatial and temporal link of gold mineralization with a specific granitoid intrusion. A contact metamorphic thermal aureole and a zonal variation of element associations /mineral assemblages in the veins around a pluton are also lacking. Moreover, the ore mineral assemblages at Flatschach are not charaterized by reduced sulfide assemblages and they are Cu-dominated and not Cu-poor as demanded for intrusion related gold deposits (Table 8).

From the geological, mineralogical and chemical characteristics the Cu-Au deposits in the Flatschach area are rather comparable with orogenic gold deposits. The similarities with this genetic class include: the convergent geotectonic setting, the link to the deformational and thermal orogenic evolution (i.e., late tectonic post-peak metamorphic vein formation), the host rocks, the regional tectonic control of ore structures (i.e., local extension structures related to large-scale compression), the sulfide gangue and alteration assemblages, and the Au:Ag ratios (Table 8).

The Flatschach vein system developed in the Austroalpine basement units and the mineralized structures are discordant and much younger than the pre-Alpine metamorphic volcano-sedimentary and intrusive host rocks. Vein orientation is controlled by Alpine regional tectonics and the veins are quartz-dominated with minor carbonate minerals (calcite, Mg-Fe-dolomite) and sulfides (pyrite, arsenopyrite). The alteration assemblages are dominated by quartz, Ca-Fe-Mg carbonates, white mica, albite and sulfides.

The element association at Flatschach includes S, As, Cu, Fe, Au, Ag, Bi, ±Hg, ±Co±Zn, ±Pb. These elements are fixed in various phases depending on the paragenetic stage. In stage 1 these are the common sulfides pyrite, arsenopyrite and chalcopyrite etc. plus gold. The ratio of Au:Ag of gold from this first stage (~4-5) falls within the range recorded for orogenic deposits. The common association of gold with chalcopyrite, arsenopyrite and pyrite in a quartz-carbonate gangue and the type of alteration (sericitization, carbonatization) indicating addition of CO_2, H_2O, S, and LIL elements during alteration is quite common in mesozonal deposits (e.g., Groves et al. 1998; Kerrich et al. 2000). Mercury is a minor constituent of gold at Flatschach. Mercury (and antimony) are more common in lower temperature orogenic deposits formed at shallower crustal depths (Groves 1993). The temperatures of ore formation for the stage 1 assemblage at Flatschach is estimated at 200–270 °C, which is at the lower temperature range of orogenic gold deposits, which can form over a considerable PT range (220–500 °C, 0.05–0.4 GPa, Table 8). Notable differences to the orogenic gold deposits in the Alps will be discussed at the end of the next chapter.

Comparison with orogenic gold deposits in the Eastern Alps

First a review of orogenic gold deposits in the Eastern Alps is given in this chapter and then features of Cu-Au mineralization at Flatschach are briefly compared to these deposits. Major historic gold production in the Eastern Alps was in the Hohe Tauern area (Paar et al. 2006). Important gold districts include the Au-(Ag)-As veins at Gastein-Rauris and in Pölla-Maltatal, the Au-(Ag)-As-Cu deposits in the Silbereck Formation (Rotgülden, Altenberg), the Au veins in the Glockner Group (Fusch valley), and the Au-(W) deposits at

the eastern margin of the Tauern Window (Schellgaden). In addition Au-Ag-As and Sb-(W) mineralization is known in the Austroalpine units, especially in the Kreuzeck- and Goldeck Mountains (Fig. 1a, Weber 2015).

The Schellgaden deposits are hosted in pre-Alpine igneous and sedimentary protoliths, and are distinguished from the typical Tauern gold veins by distinct textures (e.g., mylonitic quartz veins), mineral assemblages (gold, gold tellurides, pyrite, galena, ±sphalerite, scheelite, tourmaline), element associations (e.g., the lack of arsenic), and Pb isotope composition (Amann et al. 1997; Paar 1997). A pre-Alpine age of the earliest Au-(W) assemblage in the mylonitic quartz veins has been suggested based on a Variscan Sm-Nd errorchron age of scheelite (Wieser et al. 2011). Hence, these deposits will be excluded from further discussion.

The epigenetic gold veins ("Tauerngoldgänge") in the Gastein-Rauris area are controlled by subvertical brittle structures crosscutting the ductile metamorphic fabrics. They define about NNE-SSW to NE-SW trending vein systems (up to 7 km in length and 1 km in depth) in the Variscan metagranitoids (Central Gneiss). Partly, they also extend into the para-autochtonous Permomesozoic metasedimentary cover. Vertical zoning has been documented in some mining areas with gold-pyrite-arsenopyrite at depth grading into Pb-Zn-(Sb) rich assemblages at shallower levels (Paar 1997). Alteration is negligible, only narrow alteration zones around the veins show sericitization, silicification and sulfidation. Average gold grades are about 6–8 ppm at Gastein though gold distribution in the veins is irregular and higher ore grades (ore shoots) have been reported from the vein swells (Paar in Ebner et al. 2000). The common ore minerals are arsenopyrite, pyrite, galena, sphalerite, chalcopyrite with quartz, dolomite-ankerite, magnesite-siderite as gangue minerals. Precious metals are contained in gold having variable Ag concentration as well as in various complex Ag-Pb-Bi-(Sb-Cu) sulfosalts and in tellurides. K-Ar dating of sericite from the alteration zone yielded an age of 27 Ma (Paar 1997).

The Au-Ag-As-(Cu) mineralization in the Rotgülden area can be regarded as a subtype of the Tauern gold veins. It is structurally and lithologically controlled and hosted in polydeformed carbonate-rich metasediments of the Permomesozoic Silbereck Formation and in the underlying orthogneiss basement; in the latter they form thin extensional veins. The ores in the metasediments occur as breccia ores in shearzones preferentially at marble-mica schist contacts, in tension gashes, and as irregular metasomatic replacements (cavity fillings) within the metacarbonate layers (Horner et al. 1997). Major ore bodies are concentrated in fold hinges (saddle reefs). Chloritization is the common type of alteration. Typical ore minerals are arsenopyrite, pyrite, pyrrhotite, and chalocpyrite. Locally galena, sphalerite, and tetrahedrite-tennantite may become important. Gold is often present as inclusion in sulfides and is typically associated with Bi-minerals (bismuthinite, gustavite, matildite etc.) and tellurides (hessite, joseite etc.). Gold has variable composition (e.g., Altenberg Au/Ag=7.3–0.6, Putz et al. 2003). Two mineralization stages are present at Rotgülden: A first stage is characterized by arsenopyrite-pyrrhotite-pyrite (±gold, bismuthinite, gustavite) and formed at 370±10 °C. The second one is characterized by high-temperature chalcopyrite associated with Bi-rich minerals. Most of the gold was precipitated during the second stage, formed at ~330 °C (Horner et al. 1997; Paar 1997). Recent exploration work (Noricum Gold Limited) has shown a more complex situation with additional stages of formation, which will be investigated in detail in an ongoing project. At Altenberg the paragenetic sequence is similar. There a 3rd stage of gold with tetrahedrite, chalcopyrite, sphalerite and galena and a 4th stage with Ag-bearing galena have additionally been recognized (Putz et al. 2003).

Similar precious metal deposits are known to the south of the Tauern Window in the Austroalpine units of the Kreuzeck and Goldeck Mountains. These deposits are already located in the upper (Adriatic) plate of the Alpine orogenic wedge and include vein and shearzone-hosted Au-Ag-As and Sb-(W) mineralization (Feitzinger et al. 1995). Mineralization is linked with E-W trending semiductile to brittle strike-slip faulting related to oblique subduction during the Late Eocene to Oligocene. It is older that the Tauern gold veins for which a Late Oligocene to Early Miocene age has been proposed (Amann et al. 2002).

The ore forming fluids in the Eastern Alpine orogenic gold deposits are carbono-aqueous fluids of low salinity (<6 wt.% NaCl equiv.). Formation temperatures range between 190 °C and 420 °C for individual deposits and mineralization stages, respectively (Paar 1997). At Goldzeche, where a detailed fluid inclusion study was made (Robl and Paar 1994), several mineralization stages formed at different temperatures: arsenopyrite-gold stage (310–380 °C; 0.7–1.4 kbar), Au-Bi-rich stage (275 °C–310 °C; 0.7–0.9 kbar) and Ag-rich Pb-Zn-Cu-Sb stage (190 °C–230 °C; 0.5–0.8 kbar). At Siglitz (Imhof adit) formation conditions of 370 °C-420 °C, 0.7 to<1 kbar and 200 °C–260 °C were reported for the arsenopyrite-dominated gold stage and the Ag-dominated base metal assemblage, respectively (Pohl and Belocky 1994). Gold mineralization was explained with unmixing of low-salinity H_2O-CO_2 fluids at 200 °C–280 °C and around 1 kbar (Craw et al. 1993). Homogenization temperatures (i.e., minimum formation termperatures) of fluid inclusions from Rotgülden-Altenberg are ~310–350 °C for the Au-(Ag-Pb-Bi) stage, and ~230° for the tetrahedrite-tennantite stage (Horner et al. 1997; Putz et al. 2003). As seen from these data ore forming fluids and conditions are well comparable to those of orogenic gold deposits in the central Alps and elsewhere (Garofalo et al. 2014; Ridley and Diamond 2000).

Formation of gold veins in the Tauern Window has been related to late orogenic exhumation of the Tauern Window in

the Late Oligocene - Early Micocene during the advanced stage of continental collision and formation of the Tauern metamorphic core complex (Amann et al. 2002). Gold-mineralized tension gashes and quartz veins (older NE-SW veins overprinted by NNE-SSW veins) are among the oldest brittle structures in the Tauern Window and they formed as a result of compressional deformation (subhorizontal σ_1 oriented NE-SW rotating into NNE-SSW) related with NW-SW / WNW-ESE extension (Kurz et al. 1994). According to the scarce age data of gold mineralization in the Eastern Alps (~27 Ma, Paar 1997) vein formation only sightly post-dates the peak of Barrovian metamorphism in the southeastern Tauern Window (28–30 Ma, Inger and Cliff 1994). Hence, gold deposits started to form during the early retrograde metamorphic stage at temperatures between ~300 °C and 400 °C and evolved to lower temperatures during ongoing exhumation and cooling. Because of the lack of systematic age dating of gold deposits in the Eastern Alps it remains unclear if there was a prolonged time span (10.6 to 31.6 Ma) of ore formation and a systematic regional trend as documented in the nortwestern Alps (Pettke et al. 1999).

To some extent similarities are seen in the mineralogy between Flatschach and the other gold deposits in the Eastern Alps. The association of gold with arsenopyrite, pyrite and chalcopyrite in the early mineralization stages is typical. Other notable mineralogical differences are that Ag-Bi-Pb(Cu-Sb) sulfosalts and tellurides are exclusively present in the Tauern area whereas Cu-arsenides like domeykite and koutekite are restricted to the lower temperature ore stage at Flatschach.

As pointed out the general geodynamic setting, the structural control of mineralization, and the late orogenic timing of mineralization are also comparable. In both cases mineralized structures are controlled by local extensional structures formed in an overall compressional tectonic regime. This allowed orogenic type fluids migrating along this structural network from deeper (mantle (?) /crustal) to shallower crustal levels transporting and precipitating gold and associated metals. Future research shall clarify (1) if fluids in the Flatschach Cu-Au deposits are truly of the orogenic type and (2) to which of the two Alpine collision events (Late Cretaceous vs. Tertiary) Cu-Au mineralization at Flatschach is linked.

Conclusions

- The Cu-Au veins in Flatschach area are hosted in poly-metamorphic rocks of the Austroalpine nappe system in the upper plate of the Alpine orogen. Formation of mineralized subvertical structures post-dates Late Cretaceous peak metamorphism but was prior to the deposition of the coal-bearing Early/Middle Miocene sediments in the Fohnsdorf pull-apart basin and is tentatively related to extensional exhumation of the Seckau complex.
- Poly-stage ore formation is recognized: (a) Assemblages of the first metamorphic hydrothermal stage are similar to those of mesozonal orogenic gold deposits (~200 °C to ~270 °C). They were overprinted by a second lower temperature (70-160 °C) hydrothermal event during which Cu-rich sulfides (digenite, anilite, blue remaining covellite etc.) and the rare Cu-arsenides domeykite and koutekite formed and finally by a third stage of supergene weathering.
- Gold occurs in all three paragenetic stages. Gold of stage 1 and 2 is similar in size and composition but has different liberation characteristics. Gold from stage 3 is finer-grained and has high Ag and Hg concentrations.
- The historic copper deposits at Flatschach show some similarities to orogenic gold deposits in the Eastern Alps (e.g., Tauern gold veins) and in metamorphic terranes elsewhere but they have a predominance of Cu and lack complex sulfosalts and tellurides.
- A unique aspect of Flatschach is the presence of rare Cu-arsenides developed during the second lower temperature overprint.

Acknowledgments The authors are grateful to Universalmuseum Joanneum, namely Bernd Moser and Hans-Peter Bojar, for providing historic polished sections and ore samples from the so-called "Friedrich Archiv" at Universalmuseum. Helmut Mühlhans and Federica Zaccarini are thanked for assistance with electron microprobe analyses, Ronald Bakker for assistance with Laser Raman spectroscopy. Ralf Schuster, Alexander Schmiderer and Heinz Mali are thanked for introducing us to the field area. We thank Albert Schedl for providing unpublished maps and documents from archives of Geologische Bundesanstalt in Vienna. Gerd Rantisch is thanked for redrawing Fig. 2. Noricum Gold Ltd., namely Greg Künzel, is thanked for financing of this project and permission to publish results of an exploration project. We acknowledge the constructive reviews by L. Diamond and P. Spry.

References

Amann G, Daxner G, Neubauer F, Paar WH, Steyrer HP, Genser J, Handler R, Kurz W (1997) Structural evolution of the Schellgaden gold district, eastern Tauern Window, Austria; a preliminary report. Zentralbl Geol Palaeont Teil I 1996:215–228

Amann G, Paar WH, Neubauer F, Daxner G (2002) Auriferous arsenopyrite-pyrite and stibnite mineralization from the Siflitz-Guginock area (Austria); indications for hydrothermal activity during Tertiary oblique terrane accretion in the Eastern Alps. In: Blundell DJ, Neubauer F, von Quadt A (eds) The timing and location of major ore deposits in an evolving orogen. Geol Soc London Spec Publ 204:103–117

Barton PB (1973) Solid solutions in the system Cu-Fe-S, Part I; The Cu-S and Cu-Fe-S joins. Econ Geol 68:455–465

Bestel M, Gawronski T, Abart R, Rhede D (2009) Compositional zoning of garnet porphyroblasts from the polymetamorphic Wölz Complex, Eastern Alps. Miner Petrol 97:173–188

Craw D, Teagle DAH, Belocky R (1993) Fluid immiscibility in late-Alpine gold-bearing veins, eastern and northwestern European Alps. Mineral Deposita 28:28–36

Ebner F, Cerny I, Eichhorn R, Götzinger M, Paar W, Prochaska W, Weber L (2000) Mineral resources in the Eastern Alps and adjoining areas. Mitt Österr Geol Ges 92(1999):157–184

Faryad SW, Hoinkes G (2003) P-T gradient of Eo-Alpine metamorphism within the Austroalpine basement units east of the Tauern Window (Austria). Miner Petrol 77:129–159

Faryad SW, Melcher F, Hoinkes G, Puhl J, Meisel T, Frank W (2002) Relics of eclogite facies metamorphism in the Austroalpine basement, Hochgrössen (Speik complex), Austria. Miner Petrol 74:49–73

Feitzinger G, Paar WH, Tarkian M, Holzer H, Weinzierl G (1995) Vein type Ag-(Au)-Pb, Zn, Cu-(W, Sn) mineralization in the Southern Kreuzeck Mountains, Carinthia Province, Austria. Miner Petrol 53:307–332

Frank W, Esterlus M, Frey I, Jung G, Krohe A, Weber J (1983) Die Entwicklungsgeschichte von Stub- und Koralpenkristallin und die Beziehung zum Grazer Paläozoikum. In: Flügel H (ed) Die frühalpine Geschichte der Ostalpen, Hochschulschwerpunkt S15, Heft 4, Jahresbericht 1982, vol 4. Universität Graz, Graz, pp 263–293

Friedrich OM (1964) Die Kupfererzänge von Flatschach bei Knittelfeld. Dissertation vorgelegt 1951 von Wassil Jarlowsky. Arch Lagerst Forsch 2:32–75

Gaidies F, Abart R, De Capitani C, Schuster R, Connolly JAD, Reusser E (2006) Characterization of polymetamorphism in the Austroalpine basement east of the Tauern Window using garnet isopleth thermobarometry. J Metamorph Geol 24:451–475

Garofalo PS, Fricker MB, Guenther D, Bersani D, Lottici PP (2014) Physical-chemical properties and metal budget of Au-transporting hydrothermal fluids in orogenic deposits. In: Garofalo PS, Ridley JR (eds) Gold-transporting hydrothermal fluids in the Earth's crust, vol 402, Geol Soc London Spec Pub., pp 71–102

Goble RJ (1980) Copper sulfides from Alberta; yarrowite Cu_9S_8 and spionkopite $Cu_{39}S_{28}$. Can Mineral 18:511–518

Göd R (1987) Projekt Gold-Tremmelberg. Unpublished report, Vienna

Goldfarb RJ, Baker T, Dube B, Groves DI, Hart CJR, Gosselin P (2005) Distribution, character, and genesis of gold deposits in metamorphic terranes. 100th Anniversary Volume Society of Economic Geologists, Littleton, pp 407–450

Groves DI (1993) The crustal continuum model for late-Archaean lode-gold deposits of the Yilgarn Block, Western Australia. Miner Deposita 28:366–374

Groves DI, Goldfarb RJ, Gebre-Mariam M, Hagemann SG, Robert F (1998) Orogenic gold deposits: A proposed classification in the context of their crustal distribution and relationship to other gold deposit types. Ore Geol Rev 13:7–27

Groves DI, Goldfarb RJ, Fo R, Hart CJR (2003) Gold deposits in metamorphic belts: Overview of current understanding, outstanding problems, future research, and exploration significance. Econ Geol 98:1–29

Hart C, Goldfarb RJ (2005) Distinguishing intrusion-related from orogenic gold systems. New Zealand Minerals Conference: Realising New Zealand's Mineral Potential. Australasian Institute of Mining and Metallurgy, pp 125–133

Horner J, Neubauer F, Paar WH, Hansmann W, Koeppel V, Robl K (1997) Structure, mineralogy, and Pb isotopic composition of the As-Au-Ag deposit Rotgülden, Eastern Alps (Austria): significance for formation of epigenetic ore deposits within metamorphic domes. Miner Deposita 32:555–568

Hough RM, Butt CRM, Fischer-Bühner J (2009) The crystallography, metallography and composition of gold. Elements 5:297–302

Inger S, Cliff RA (1994) Timing of metamorphism in the Tauern Window, Eastern Alps; Rb-Sr ages and fabric formation. J Metamorph Geol 12:695–707

Jarlowsky W (1951) Die Kupfererzgänge von Flatschach bei Knittelfeld. PhD thesis Montanuiversität Leoben

Kerrich R, Goldfarb R, Groves D, Garwin S, Jia Y (2000) The characteristics, origins, and geodynamic settings of supergiant gold metallogenic provinces. Sci China Sers D 43:1–68

Kretschmar U, Scott SD (1976) Phase relations involving arsenopyrite in the system Fe-As-S and their application. Can Mineral 14:364–386

Kurz W, Neubauer F, Genser J, Horner H (1994) Sequence of Tertiary brittle deformations in the Eastern Tauern Window (Eastern Alps). Mitt Österr Geol Ges 86(1993):153–164

Leitner T (2013) Gold in the historic copper deposits at Flatschach, Styria. Master thesis, Montanuniversitaet Leoben

Melcher F, Meisel T (2004) A metamorphosed early Cambrian crust–mantle transition in the Eastern Alps, Austria. J Petrol 45:1689–1723

mindat.org the mineral and locality data base. www.mindat.org. Accessed Mar 2015

Morey AA, Tomkins AG, Bierlein FP, Weinberg RF, Davidson GJ (2008) Bimodal distribution of gold in pyrite and arsenopyrite; examples from the Archean Boorara and Bardoc shear systems, Yilgarn Craton, Western Australia. Econ Geol 103:599–614

Neubauer F, Frisch W, Schmerold R, Schlöser H (1989) Metamorphosed and dismembered ophiolite suites in the basement units of the Eastern Alps. Tectonophysics 164:49–62

Neubauer F, Frisch W, Hansen BT (2002) Early Palaeozoic tectonothermal events in basement complexes of the eastern Greywacke Zone (EasternAlps): evidence from U-Pb zircon data. Int J Earth Sci 91:775–786

Noricum Gold Limited. Company homepage www.noricumgold.com. Accessed Apr 2014

Paar WH (1997) Edelmetalle. In: Weber L (ed) Handbuch der Lagerstätten der Erze, Industrieminerale und Energierohstoffe Österreichs Erläuterungen zur metallogenetischen Karte von Österreich 1 : 500000 unter Einbeziehung der Industrieminerale und Energierohstoffe, Arch Lagerst Forsch Geol B-A 19:276–284

Paar WH (2014) Unpublished report for Noricum Gold AT, 2 pp

Paar WH, Meixner H (1979) Neues aus den Kupfererz-Gängen des Flatschacher Bergbau-Reviers in Knittelfeld, Steiermark. Der Karinthin 81:148–150

Paar W, Günther W, Gruber F (2006) Das Buch vom Tauerngold.- 2. aktualisierte, mit zahlreichen Ergänzungen versehene Auflage. Verlag Anton Pustet, Salzburg

Pettke T, Diamond LW, Villa IM (1999) Mesothermal gold veins and metamorphic devolatilization in the northwestern Alps; the temporal link. Geology 27:641–644

Pfingstl S, Kurz W, Schuster R, Hauzenberger C (2015) Geochronological constraints on the exhumation of the Austroalpine Seckau Nappe (Eastern Alps). Austrian J Earth Sci 108:172–185

Pohl W, Belocky R (1994) Alpidic metamorphic fluids and metallogenesis in the Eastern Alps. Mitt Österr Geol Ges 86(1993):141–152

Posfai M, Buseck PR (1994) Djurleite, digenite, and chalcocite; intergrowths and transformations. Am Mineral 79:308–315

Punzengruber K, Polegeg S, Scherer J (1977) Geochemische Untersuchung von Bachsedimenten im Kristallin nördlich von Knittelfeld und ihre Bedeutung für die Lagerstättensuche. Berg- und Hüttenmänn Monatsh 122:5

Putz H, Paar WH, Topa D, Horner J, Lüders V (2003) Structurally controlled gold and sulfosalt mineralization: the Altenberg example, Salzburg Province, Austria. Miner Petrol 78:111–138

Ramdohr P (1975) Die Erzmineralien und ihre Verwachsungen, 4th edn. Akademie-Verlag, Berlin

Ridley JR, Diamond LW (2000) Fluid chemistry of orogenic lode gold deposits and implications for genetic models. Rev Econ Geol 13: 141–162

Robl J, Paar WH (1994) Fluid-Inclusion Untersuchungen an Golderzen der Goldzeche, Sonnblickgruppe, (Hohe Tauern, Kärnten). Mitt Österr Mineral Ges 139:151–158

RRUFF http://rruff.info. Accessed 2013

Sachsenhofer RF, Kogler A, Polesny H, Strauss P, Wagreich M (2000) The Neogene Fohnsdorf Basin: basin formation and basin inversion during lateral extrusion in the Eastern Alps (Austria). Int J Earth Sci 89:415–430

Scharbert S (1981) Untersuchungen zum Alter des Seckauer Kristallins. Mitt Ges Geol Bergbaustud Österr 27:173–188

Schermaier A, Haunschmid B, Finger F (1997) Distribution of Variscan I- and S-type granites in the Eastern Alps; a possible clue to unravel pre-Alpine basement structures. In: Neubauer F, Cloetingh S, Dinu C, Mocanu V (eds) Tectonics of the Alpine-Carpathian-Pannonian region. Elsevier, Amsterdam, pp 315–333

Schmid SM, Fügenschuh B, Kissling E, Schuster R (2004) Tectonic map and overall architecture of the Alpine orogen. Eclog Geol Helvet 97: 93–117

Schuster R (2011) Ostalpin. In: Rupp C, Linner M, Mandl G (eds) Geologische Karte von Oberösterreich 1:200000. Erläuterungen, Geologische Bundesanstalt, Wien, pp 61–67

Schuster R, Stüwe K (2008) Permian metamorphic event in the Alps. Geology 36:603–606

Sharp ZD, Essene EJ, Kelly WC (1985) A re-examination of the arsenopyrite geothermometer; pressure considerations and applications to natural assemblages. Can Mineral 23:517–534

Skinner BJ, Luce FD (1971) Stabilities and compositions of alpha-domeykite and algodonite. Econ Geol 66:133–139

Strauss P, Wagreich M, Decker K, Sachsenhofer RF (2001) Tectonics and sedimentation in the Fohnsdorf-Seckau Basin (Miocene, Austria); from a pull-apart basin to a half-graben. Int J Earth Sci 90:549–559

Tectonics FP software http://www.tectonicsfp.com

Tenczer V, Stuewe K (2003) The metamorphic field gradient in the eclogite type locality, Koralpe region, Eastern Alps. J Metamorp Geol 21:377–393

Thöni M (1999) A review of geochronological data from the Eastern Alps. Schweiz Mineral Petrogr Mitt 79:209–230

Weber L (2015) IRIS Interaktives Rohstoff-Informations-System. Geologische Bundesanstalt, http://geomap.geolba.ac.at/IRIS/einstieg.html

Whiteside LS, Goble RJ (1986) Structural and compositional changes in copper sulfide during leaching and dissolution. Can Mineral 24: 247–258

Whitney DL, Evans BW (2010) Abbreviations for names of rock-forming minerals. Am Mineral 95:185–187

Wieser B, Raith JG, Thöni M, Cornell DH, Stein H, Paar W (2011) In-situ trace element and ID-TIMS Sm-Nd analysis of scheelite and Re-Os dating of molybdenite at Schellgaden, a Au-(W) deposit in the Estern Alps, Austria. Pangeo, 2010 Abstracts. J Alpine Geol 52: 253–254